Formation of Isolated Radio Type II Bursts at Low Frequencies

Silja Pohjolainen[1] [ID] · **Nasrin Talebpour Sheshvan[2]** [ID]

Abstract

The first appearance of radio type II burst emission at decameter-hectometer (DH) waves typically occurs in connection, and often simultaneously, with other types of radio emissions. As type II bursts are signatures of propagating shock waves that are associated with flares and coronal mass ejections (CMEs), a rich variety of radio emissions can be expected. However, sometimes DH type II bursts appear in the dynamic spectra without other or earlier radio signatures. One explanation for them could be that the flare-CME launch happens on the far side of the Sun, and the emission is observed only when the source gets high enough in the solar atmosphere. In this study we have analysed 26 radio type II bursts that started at DH waves and were well-separated ('isolated') from other radio emission features. These bursts were identified from all DH type II bursts observed in 1998 – 2016, and for 12 events we had observations from at least two different viewing angles with the instruments on board Wind and the Solar Terrestrial Relations Observatory (STEREO) satellites. We found that only 30% of the type II bursts had their source origin on the far side of the Sun, but also that no bursts originated from the central region of the Sun (longitudes E30 – W40). Almost all of the isolated DH type II bursts could be associated with a shock near the CME leading front, and only few were determined to be shocks near the CME flank regions. In this respect our result differs from earlier findings. Our analysis, which included inspection of various CME and radio emission characteristics, suggests that the isolated DH type II bursts could be a special subgroup within DH type II bursts, where the radio emission requires particular coronal conditions to form and to die out.

1. Introduction

The first discovery of solar radio type II bursts dates back to 1947, by Payne-Scott, Yabsley, and Bolton (1947). Type II bursts appear as continuous and slowly drifting bursts, from high

---

✉ S. Pohjolainen
   silpoh@utu.fi

✉ N. Talebpour Sheshvan
   natash@utu.fi

1   Tuorla Observatory, Department of Physics and Astronomy, University of Turku, Turku, Finland

2   Space Research Laboratory, Department of Physics and Astronomy, University of Turku, Turku, Finland

to low frequencies, in the radio dynamic spectra (Wild and McCready, 1950). The frequency drift was then found to display the decreasing electron density in the solar atmosphere, and the discovery of harmonics was taken as evidence that there was a common source producing oscillations at a fundamental plasma frequency and its second harmonic; see for example the historic review by Pick and Vilmer (2008). The disturbance producing type II emission was later identified as an MHD shock (Uchida, 1960).

Type II bursts can be categorized into metric (m), decameter hectometric (DH), and kilometric (km), based on the wavelengths they are observed. DH waves cover the frequency range of 30 MHz – 300 kHz, but as radio emission below $\approx$ 25 MHz is blocked by the Earth's atmosphere the whole wavelength range cannot be observed with ground-based instruments. The existing space instruments have instrumental upper limits at 16 MHz (Solar Terrestrial Relations Observatory, STEREO) and 14 MHz (Wind), and so it is customary to define DH and interplanetary (IP) type II bursts as those that occur at frequencies below these space instrument upper limits.

Previous studies have shown that DH and km type II bursts are produced by coronal mass ejection (CME) driven shocks (Sheeley et al., 1985; Cane, Sheeley, and Howard, 1987; Gopalswamy et al., 2001). CMEs are large-scale plasma structures ejected from the solar chromosphere and corona, and these transients propagate out to the IP space. In shock theory, a shock can form as a bow shock at the leading front of the CME, as a driven shock near the CME front (even well-separated from the driver after launch), or as a driven (expansion) shock near the CME flanks; see for example the reviews by Warmuth (2007) and Vrsnak and Cliver (2008).

A bow shock is formed when the speed of a coronal transient exceeds the local magnetosonic speed, which in the solar corona is well represented by the Alfvén speed. A model of the magnetic field of an active region gave as a result a local Alfvén speed minimum at a distance of $1.2 - 1.8$ solar radii ($R_\odot$), and a maximum of 740 km s^{-1} at a distance of 3.8 $R_\odot$ (Mann et al., 2003). The model by Warmuth and Mann (2005) found a local speed minimum at the coronal base, 300 km s^{-1}, and a local maximum at a distance of 3.5 $R_\odot$, 1100 km s^{-1}. For example Evans et al. (2008) have compared the Alfvén speed values obtained for different types of regions (open field regions, streamers, active regions) with the different models and techniques. Due to the high magnetosonic speed, most metric type II bursts do not continue into the outer corona. Besides, as the magnetosonic speed decreases at distances larger than $3.5 - 3.8$ $R_\odot$, DH type bursts are more likely to form there. This distance corresponds to a frequency of $8 - 12$ MHz in most coronal density models; see for example the comparison between heights and frequencies in Pohjolainen et al. (2007).

The characteristics of CMEs associated with DH type II bursts have been well-studied and reported (Gopalswamy, 2000; Gopalswamy et al., 2001, 2002; Sharma et al., 2008; Pappa Kalaivani et al., 2010), and also the differences between radio-loud and radio-quiet CMEs have been investigated (Gopalswamy et al., 2010). Basically, CMEs associated with DH type II bursts have been found to be faster and wider. In addition, Vasanth and Umapathy (2013) found that in the DH type II burst-associated events, CME properties like speed, width, and shock speed were higher in limb events than in disc events, suggesting that projection effects play a part in the measurements.

Also DH type II bursts have been studied statistically, by their start and end frequencies, their duration, burst source location, and emission bandwidth. Sharma and Mittal (2017) concluded that the average duration of bursts that started between 16 and 1 MHz was considerably less than those that started below 1 MHz. In their analysis of type II burst end frequencies, Vasanth et al. (2015) concluded that the lower the emission end frequency, the higher the possibility of having a strong geomagnetic storm near Earth. Shanmugaraju et al. (2018)

divided the type II bursts into groups by their end frequency: (A) higher than 1 MHz, (B) intermediate, between 1 MHz and 100 kHz, and (C) lower than 100 kHz. Their analysis indicated that there was a correlation between the observed CME height and the estimated type II burst height for groups B and C, but no correlation for group A. They suggested that the type II shock could occur at the flanks of the CME in group A, and at the CME leading front in groups B and C. The statistical results obtained by Aguilar-Rodriguez et al. (2005) showed that the average bandwidth-to-frequency ratio was ≈ 0.3 in the DH type II bursts observed with the Wind/Radio and Plasma Wave Investigation (WAVES) radio instruments, irrespective of their spectral domain. The ratio distribution, however, covered a large interval of $0.05 - 0.8$, indicating that in individual bursts the emission bandwidth can be quite different.

The DH type II burst appearances have also been used to classify events. Pohjolainen, Allawi, and Valtonen (2013) selected wide-band and diffuse IP type II bursts to find where they originated. Most of the analysed bursts (and shocks) could be considered to be due to plasma emission, formed at or just above the CME leading edge. However, for some radio events the source was unclear and could have been due to other mechanisms, like Bastian (2007) had earlier suggested.

DH type II bursts are typically observed in the radio dynamic spectra mixed with other strong emissions like type III bursts (fast electron beams), but they can also appear quite suddenly and without other close-in-time radio features. Some of these well-separated, isolated DH type II bursts can be easily explained by their source location: If the flare-CME launch happens on the far side of the Sun, radio emission would be observed only when the radio emission source gets high enough in the solar atmosphere, where the emission is no longer blocked by the solar disc or by the dense solar atmosphere, i.e., where the emission frequency exceeds the local plasma frequency. Observation of accelerated electron beams would then depend on the direction of the magnetic field lines. For type II bursts, the propagation direction and wideness of the shock front could also play a part.

Our study presents an analysis of selected DH type II radio bursts that were observed well-separated from other radio emission features. With the statistical analysis of the burst, flare, and CME characteristics we try to determine the reasons for them to appear isolated in the radio dynamic spectra, and discuss their appearances and source origins. Some of the most interesting events are analysed in more detail.

2. Data Analysis

We have selected radio type II bursts that appear to start at a low frequency, at decameter-hectometer (DH) wavelengths, and which can be identified as separate structures from any other emission feature visible in the radio spectrum at that time. The type II bursts were searched using the Wind/Plasma and Radio Waves (WAVES) type II lists at https://solar-radio.gsfc.nasa.gov/wind/data_products.html and the type II list at https://cdaw.gsfc.nasa.gov/CME_list/radio/waves_type2.html, including the years 1998 – 2016.

Coronagraph images and CME leading front heights were obtained from the Large Angle and Spectrometric Coronagraph (LASCO) CME Catalog, maintained at the Coordinated Data Analysis Workshop (CDAW) Data Center. This catalogue contains data from both the Solar and Heliospheric Observatory (SOHO) and the Solar Terrestrial Relations Observatory (STEREO) missions, with white-light coronagraph images and EUV images at several different wavelengths. Solar flare data were obtained from the NOAA Satellite and Information Service (NESDIS) website. Information on radio type II bursts at meter

wavelengths were obtained from the NOAA radio spectral listings (up to year 2011), and from individual spectral plots from different radio observatories, mainly from the Radio Solar Telescope Network (RSTN) at https://www.ngdc.noaa.gov/stp/space-weather/solar-data/solar-features/solar-radio/rstn-spectral/.

For the type II burst height estimates we used the 'hybrid' atmospheric density model by Vrsnak, Magdalenic, and Zlobec (2004). As the plasma frequency f_p depends only on the plasma density n_e ($f_p = 9000\sqrt{n_e}$, when the frequency is in Hz and n_e is in cm^{-3}), the type II emission frequency can be converted to source height if we know how the density changes in the corona and interplanetary space; see for example Pohjolainen et al. (2007). Only fundamental emission lanes were used for the calculations. As at DH wavelengths fundamental emission should be stronger than the harmonic (Lengyel-Frey, Stone, and Bougeret, 1985), we assumed fundamental emission in events that showed only one emission lane.

2.1. Selection Criteria and Visual Appearances

Our selection criterion for the DH type II bursts was that the emission lane (or lanes, if both fundamental and harmonic lanes were visible) must appear below 16 or 14 MHz (instrumental upper limits), must be separated from any other radio emission feature, and must show a frequency drift in order to verify it really is a type II burst. With these criteria we excluded events with separate multiple emission lanes (fundamental-harmonic bursts accepted but mixed multiple bursts excluded), and also excluded lanes where the start of the type II burst was superposed or mixed with any other type of burst activity. For example intense type III bursts usually make it impossible to identify the actual type II start time and frequency. For data analysis purposes we also demanded that adequate CME data were available for each event. We found 26 such events from the years 1998-2016; see Table 1 in the Appendix.

A visual inspection of the spectral events showed different appearances. Some of the bursts were very short (duration $5-8$ min) and some were long-duration events that were visible for hours. Some showed narrow-band emission ($\Delta f/f \leq 0.1$) and some were very wide-band ($\Delta f/f > 0.3$). Some showed only one emission lane and some showed two emission lanes, where the second lane appeared at twice the frequency of the first. One lane events were interpreted to be due to fundamental plasma emission (F), and two-lane events due to fundamental and harmonic (F+H) plasma emission. Examples of the burst appearances are shown in Figure 1. The type II burst duration, emission band, and F and F+H appearance are listed in Tables 1 and 2, together with other burst characteristics and associated features. The radio spectra of all events are shown in the Appendix, in Figures $15-40$.

2.2. Correlation Analysis

The DH type II bursts were associated with 9 GOES M-class flares, 7 C-class flares, 3 eruptive prominences (EP), and 7 had their origin behind the limb, on the far side of the Sun, so that flare classification for them was not available.

All the DH type II bursts were associated with a close-in-time CME. CME speeds were determined at the time of the DH type II burst appearance, using the second order fits to the CME leading front heights listed in the LASCO CME Catalog. The CME speeds ranged from 480 to 1800 km s^{-1}. Of the CMEs, 9 were accelerating, 14 were decelerating, and 3 had a constant speed.

In Figure 2 we compare the source longitude (i.e., the location of the active region from where the eruption originated) with the projected CME speed, CME height at the type II start time, type II start frequency, and type II burst duration. Figure 2 shows that near the
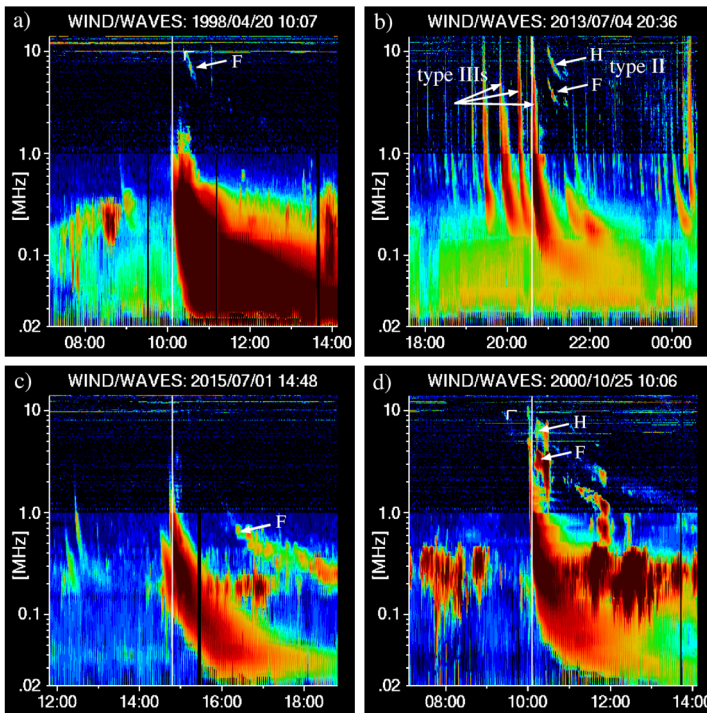
Figure 1 Examples of isolated type II bursts at DH wavelengths. **a**) A short-duration type II burst with one single lane appears at 10:25 UT at 10 MHz start frequency on 20 April 1998. **b**) A short-duration type II burst with fundamental (F) and harmonic (H) emission lane pair at 5 and 10 MHz appears at 20:57 UT on 4 July 2013. The spectrum also shows earlier type III bursts (fast-drift bursts that are formed by propagating electron beams). **c**) A long-duration type II burst with one single lane appears at 16:22 UT with a low-frequency start at 700 kHz on 1 July 2015. **d**) A strong type II burst with F and H emission lane pair appears at 4 and 8 MHz at 10:00 UT on 25 October 2000.

disc center, inside E30 – W42 longitudes there are no isolated DH type II bursts. Within the longitudes E50 – E30 and W42 – W50 all the isolated type II bursts are single (F) lane events.

The highest CME speeds are observed when the flare/CME source longitudes are $\gtrsim 90$ degrees. It may be that the observed CME speeds for the on-the-disc events suffer from projection effects and look to be lower than the real speeds, as was suggested by Vasanth and Umapathy (2013). Comparison between the CME height at the time of the type II burst start and the source longitude gives a similar result as the comparison to the CME speed.

The type II start frequency does not seem to have a clear correlation with the source longitude, but the highest start frequencies are in bursts that have their source origin near the solar limb.

The comparison between the type II emission duration and the source longitude shows that the type II events that originate near or behind the solar limb have the longest durations. Our sample of events shows quite an opposite tendency compared to that of Mittal and Verma (2017), who found that the durations of the DH type II radio bursts located at the solar disc center are longer than the durations of the bursts located at the solar limb. However, their sample of 426 DH type II bursts and our sample of 26 bursts are not directly comparable, so ours could be a selection effect.
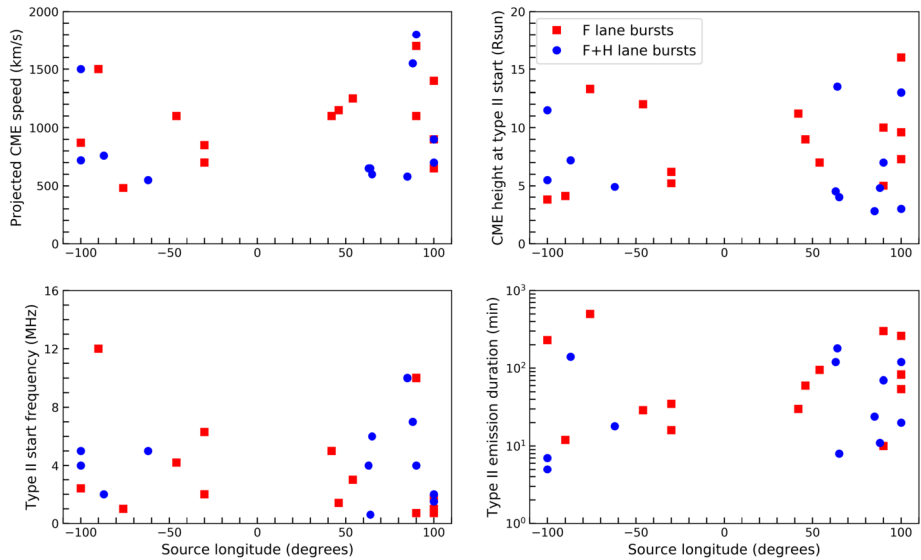
Figure 2 Flare/CME source longitude on the solar disc compared with the projected CME speed (*top left*), the CME height at the time of the type II burst start (*top right*), the type II burst start frequency (*bottom left*), and the type II burst duration (*bottom right*). Behind-the-limb events are given as -100 (behind the eastern limb) and +100 (behind the western limb). F and F+H lane bursts are plotted with different symbols.

Figure 3 shows the type II burst start frequency compared to the type II burst duration. This plot is in accordance with the finding of Sharma and Mittal (2017), that bursts starting at lower frequencies have longer durations. We also compared the projected CME leading front height at the time of the type II start with the type II burst duration, and this shows a tendency that the higher the CME is at the type II burst start, the longer the type II burst duration.

The DH type II burst start frequency does not look to have any clear correlation with the projected CME speed. When the projected CME speed is compared to the type II burst duration, we see that the highest speed CMEs do not produce long-duration DH type II bursts.

We then compared the CME angular width with the source longitude and the type II burst start frequency in Figure 4. The CME Catalog lists the associated CMEs as full halos (10/26), partial halos (13/26), and with widths 94 – 101 degrees (3/26). We measured the CME widths near the time of the type II emission start, which gave more narrow widths that ranged from 40 to 230 degrees. The smallest CME angular widths were in the events that occurred at or behind the solar limb. The closer to the disc center the event originated, the larger the angular width. This could be a simple projection effect.

A large CME angular width looks to correlate with a low type II start frequency (i.e., high formation height). However, a narrow CME width does not look to imply a high type II formation height, as some of the very narrow CMEs were associated with bursts that had a very low start frequency. This may rule out the assumption that type II burst formation requires a certain angular width for the CME.

We also compared the projected CME speed with the GOES soft X-ray maximum flux. Of the 26 events three were eruptive prominences without an observed X-ray flare and seven
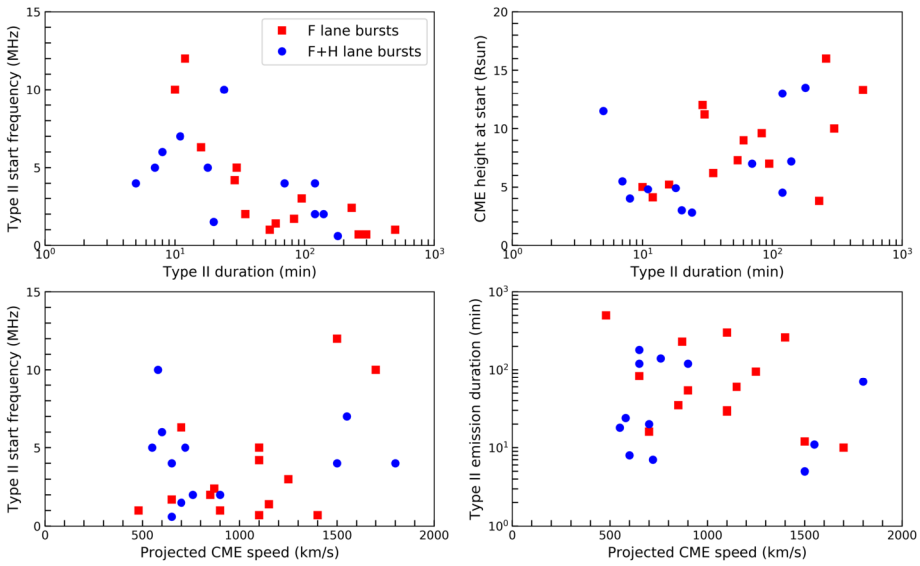
Figure 3 Type II burst duration compared with the type II burst start frequency (*top left*) and the CME height at the time of type II start (*top right*). Projected CME speed at the time of type II burst start compared with the type II burst start frequency (*bottom left*) and the type II burst duration (*bottom right*).
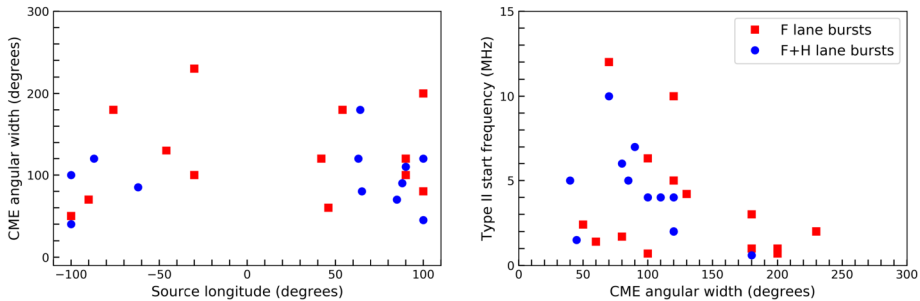

Figure 4 CME angular width near the time of type II start compared with the flare/CME source longitude (*left*) and the type II start frequency (*right*).

were far side events where GOES intensity could not be measured. The correlation plot (not shown here) suggested that the more intense the flare flux, the higher the CME speed.

Furthermore, we checked if these events showed any metric type II emission, to see if a propagating shock existed already at lower coronal heights. Due to the atmospheric cut-off in ground-based radio observations (that are possible down to $30-25$ MHz) and the instrumental limit of space observations (start frequency $16-14$ MHz), type II emission lanes that start at meter waves cannot be followed directly to DH waves, because of the spectral gap in observations. Of the analysed events, 10 out of 26 were associated with earlier metric type II emission; see Table 2. It is obvious that far side events and eruptive prominences lack metric emission. An association to flare intensity and CME speed was also noted; in our data set metric type II bursts required an M-class GOES flare and/or a very high speed CME ($1100-1800$ km s^{-1}).

Figure 5 Flare/CME source longitude on the solar disc compared with the height difference between the CME leading front and the type II burst source at the time of the type II burst start (positive when the CME is higher than the type II burst). Solid lines mark the $\pm 2\,R_\odot$ error margin for calculated heights (mainly from density models) and dashed lines indicate the values that we concluded to be within acceptable height errors in individual events.
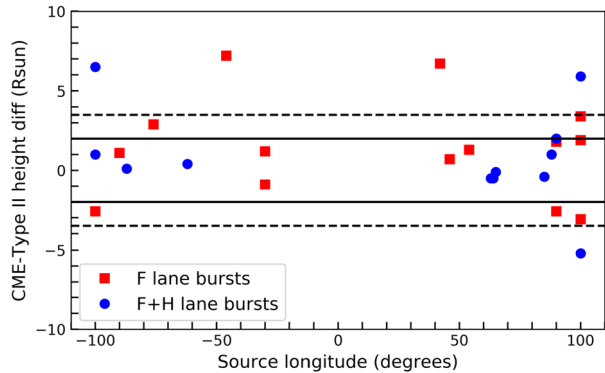
Our events were also compared with the solar energetic particle (SEP) event catalogue by Paassilta et al. (2017) that covers the years in our list. A match was found in five events. In three events (20 April 1998, 25 October 2000, 17 July 2012) the SEP injection time, determined with the velocity dispersion analysis (VDA) method, matched well with the time of the DH type II burst appearance. In two events (22 August 2005, 1 July 2015) the SEP injection time was earlier, but could be explained with an earlier metric type II burst. Due to the small number of SEP events, no further correlation analysis was performed. We note, however, that considering the spectral structures of type II bursts may help to improve the SEP forecasting accuracy (Iwai et al., 2020).

3. Events with Large Height Difference Between the CME Leading Front and the Type II Burst Source

To evaluate where our DH type II bursts could be formed, we calculated the height difference between the CME leading front and the type II burst source for each event. These are listed in Table 1. Figure 5 shows the height difference versus source longitude, and the value is positive when the CME front is located higher than the type II burst source.

Errors in type II burst height estimation can be quite large, as the calculated heights depend on the chosen atmospheric density model and on the selected frequency within the emission lane taken for calculation (for example, center or leading edge of the lane, affected also by the wideness of the emission lane). In the frequency range of $10-1$ MHz, the height difference that comes from using different (but generally accepted) density models is $\approx 2\,R_\odot$; see for example the height values in Table 1 in Pohjolainen et al. (2007).

Equally, the CME leading front height can be uncertain, especially if the front consists of a bright flux rope and a diffuse faint region ahead of it. The diffuse region has often been identified as the CME-driven shock front; see Schmidt et al. (2016b) and the references therein. Usually, the shock is more visible toward the flank regions of the CME, and the stand off distance between the shock and the CME leading edge is not more than $1-2\,R_\odot$ in this height range (Schmidt et al., 2016a), and often much less (Lee et al., 2017).

Of our 26 events, 16 could be considered to be a match between the type II burst height and the CME leading front height, within the possible $\pm 2\,R_\odot$ error. Similar heights suggest that the type II burst was most probably created by a CME bow shock.

Of the remaining ten events, five had an intermediate height difference of $2.6-3.4\,R_\odot$. These events showed relatively wide emission lanes. Wide-band emission is tricky in a sense

that the frequency selected for height calculation (lower border, lane center, or some other point inside the lane) will have a large effect on the height. The spectral plots of these events show how the frequency drift of the type II burst follows that of the CME quite well, but due to the wideness of the emission lane the heights calculated from the lane center do not always match the CME heights. Hence, some other frequency points within the emission lane could still give a good match. We also noted that in many of these events the type II height at the start of the burst was different from the CME leading front height, but later on the heights became similar. Based on our analysis, we conclude that also the five type II bursts with intermediate height differences can reasonably well be associated with the CME leading fronts.

The height difference between the CME leading front and the type II shock was observed to be very large, $5.2 - 7.2 \, R_\odot$, in five events. On 27 March 2012, the type II burst source was located $5.2 \, R_\odot$ higher than the leading front of the CME. In the other four events, the type II burst sources were located lower than the leading front of the CME. We now examine the possible reasons for these large height differences.

3.1. Event on 27 March 2012

On 27 March 2012 the DH type II burst source was located $5.2 \, R_\odot$ higher than the leading front of the main CME, which was propagating toward the west at a speed of $700 \, \text{km s}^{-1}$ at the time when the type II burst appeared (dashed line marked CME WEST in Figure 6, here the CME heights have been converted to frequencies). The CME heights were also verified from the STEREO-A/COR1 observations, and they were not higher than what was observed by SOHO/LASCO. The active region (AR) was most probably NOAA AR 11440, which had rotated to $\approx$ W100, as it was last observed from Earth on 26 March at location S25W91.

After a closer inspection, there were two earlier-launched faint and narrow CMEs which were catalogued as very poor events, and did not show up in the coronagraph images at the time of the type II burst appearance. The first one propagated toward the west (dash-dotted line marked CME WEST, the heights have been extrapolated onward from the last observed height of $4.5 \, R_\odot$ at 19:00 UT), and the second one toward the east (marked CME EAST) in Figure 6. The heights of CME EAST are near the heights of the type II burst harmonic emission. However, as STEREO-B/WAVES did not record a type II burst at all, and only one type III burst was visible below 700 kHz, it does not look probable that the CME EAST could have created the burst recorded by Wind/WAVES and STEREO-A/WAVES.

STEREO-A/WAVES dynamic spectrum shows that the radio enhancements, which we interpreted as type II F+H lanes, were located along type III burst emission lanes that were not visible in the Wind/WAVES spectrum. The radio dynamic spectrum at $180 - 25 \, \text{MHz}$ from RSTN Sagamore Hill (Earth view, same as for Wind) does not show any metric type III or type II radio emission within the time range.

We therefore conclude that the association of the type II burst to the westward propagating fast (main) CME is questionable. It is possible that the type II-like structures were not a type II burst, but flare-accelerated electrons propagating through the dense (earlier) CME structures, i.e., they were type III burst enhancements when the beams traveled through local turbulent plasma. Fundamental-harmonic structures can occur also in type III bursts, as a significant number of type III bursts at meter and decameter waves have been found to show harmonics; see for example Robinson and Cairns (1998) and the references therein.

3.2. Event on 11 December 2001

The DH type II burst on 11 December 2001 showed relatively weak emission but had a clear start at 12:45 UT, with fundamental and harmonic emission lanes (Figure 7). After 14:00
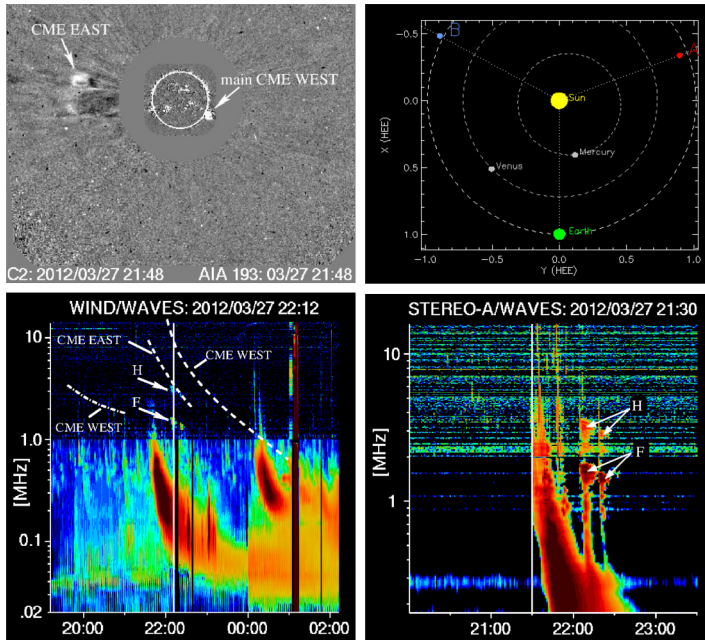
Figure 6 Event on 27 March 2012, source origin at SW90b (on the far side). The type II burst source is located 5.2 R$_\odot$ higher than the leading front of the main CME (CME WEST, dashed white line). There are earlier faint and narrow CMEs that propagate toward the west (CME WEST, dash-dotted white line) and toward the east (CME EAST, dashed white line). STEREO-A dynamic spectrum shows how radio type III emission lanes cross the features that were interpreted as type II emission. Some parts of these type III bursts are visible in the Wind/WAVES and STEREO-B/WAVES spectrum, but only at frequencies below 1 MHz. The positions of both STEREO spacecraft on 27 March 2012 are also shown. Wind/WAVES was located in L1, along the Sun-Earth line.

UT there is uncertainty if and how the lane continues, narrow or wide, as we see enhanced emission at a much wider frequency range. However, some of these enhancements could be due to type III bursts.

The main CME was located 5.9 R$_\odot$ higher than the type II burst source at 12:45 UT, but a second bright structure had appeared inside the main CME at 11:30 UT. It propagated to the same westward direction, at a speed of 500 km s^{-1}. The height evolution of the main CME and the later, inner CME structure are shown in Figure 7, indicated with white dashed lines in the dynamic spectrum. The type II burst shows a curved structure, and a similar change is observed in the height evolution of the later CME structure (height–time plot in Figure 7). The height difference between this later CME front and the type II burst is ≈ 2 R$_\odot$, which falls inside the error margin in height estimation.

We therefore conclude that the DH type II burst was created by the later CME structure, and that the curved type II structures were due to density changes along the CME propagation path, caused by the earlier (main) CME.

3.3. Events on 22 December 2002 and 31 December 2004

The DH type II burst events on 22 December 2002 and 31 December 2004 look very similar (Figure 8). Both were on-the-disc events that showed EUV dimmings. The associated GOES
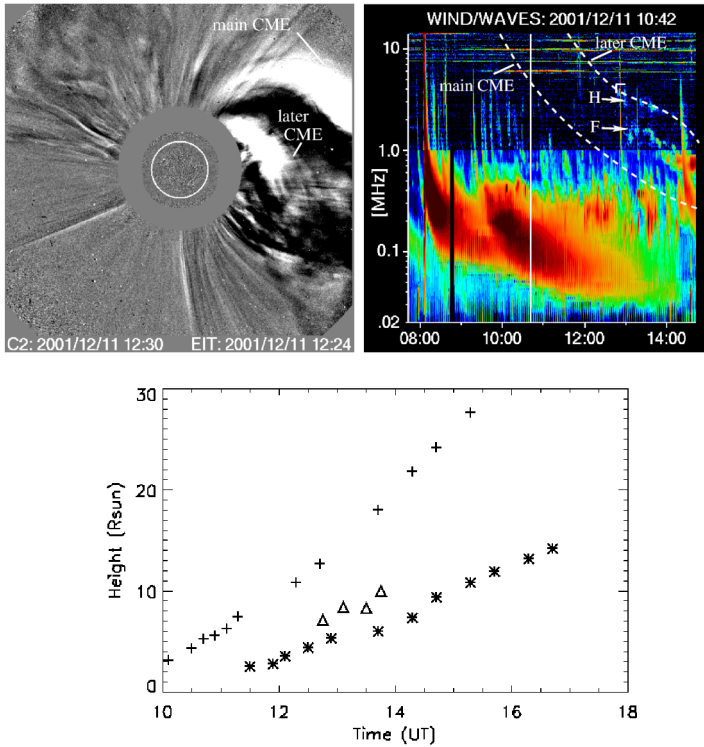
Figure 7 Event on 11 December 2001, source location at SW90b (on the far side). The leading front of the main CME is located 5.9 R$_\odot$ higher than the type II burst source. However, there is a later CME propagating westward, in the wake of the main CME. The LASCO C2 difference image (*top left*) shows the northern edge of the main CME and the leading front of the later CME. The CME propagation heights, converted to frequencies, are indicated with the dashed white lines in the radio dynamic spectrum (*top right*). The height–time plot (*bottom*) shows the height evolution of these two CME fronts (crosses and stars) and the calculated type II burst heights from the fundamental emission lane (triangles).

flares were class M1.1 and M4.2, and the flare/CME source locations were N23W42 and N04E46, respectively. The CME speed at the type II start was 1100 km s^{-1} in both events. The durations of the type II emission were 30 and 29 minutes, the type II formation heights were 4.5 and 4.8 R$_\odot$, and the respective CME heights were 11.2 and 12.0 R$_\odot$. The height differences were 6.7 and 7.2 R$_\odot$, respectively.

In both events there was strong type II burst activity at metric wavelengths (Figure 8, top panels), starting near 140 MHz and continuing down to 25 MHz (observational limit for ground-based observations, RSTN Learmonth). In both cases the metric type II emission was band-split: on 22 December 2002 at the start the fundamental frequency was split to 34 and 39 MHz and the harmonic to 68 and 78 MHz, and on 30 December 2004 split lanes can be identified to start at 80 and 100 MHz. The 30 December 2004 spectrum is more complicated, for example at 22:25 UT a separate lane is observed to start at 30 MHz but due to the observational limit it cannot be followed below 25 MHz. We calculated the radio source heights using the lower split lanes.

The height–time plots in Figure 9 show that the metric type II burst heights are in line with the CME heights, but the later DH type II burst sources are at much lower heights. The
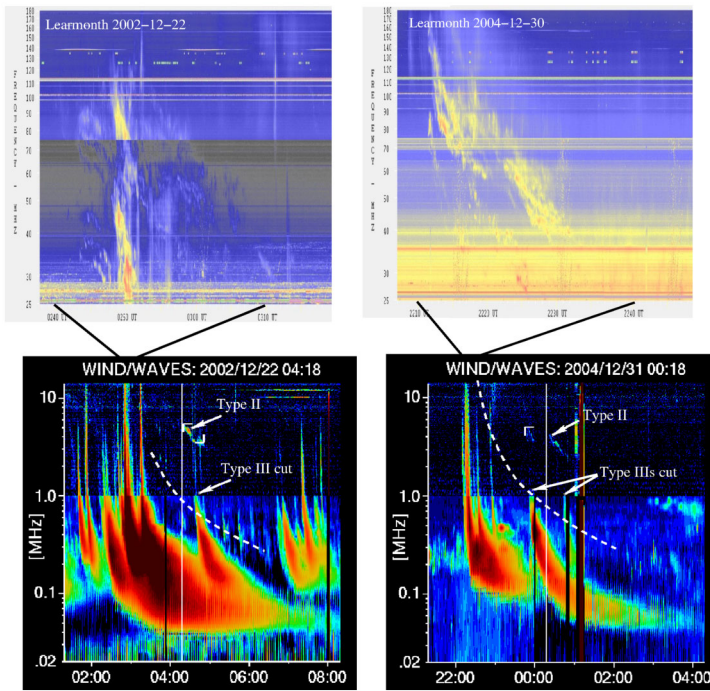
Figure 8 On 22 December 2002, the burst source origin is at N23W42. The leading front of the CME (dashed white line, *bottom left*) is located 6.7 R$_\odot$ higher than the type II burst source. On 31 December 2004, the burst source origin is at N04E46. The leading front of the CME is located 7.2 R$_\odot$ higher than the type II burst source (*bottom right*). The DH type III bursts along the CME propagation paths were 'cut', i.e., their emission did not cross the whole spectral range. Both events showed also metric type II burst activity at 140 – 25 MHz, observed by the RSTN Learmonth station.
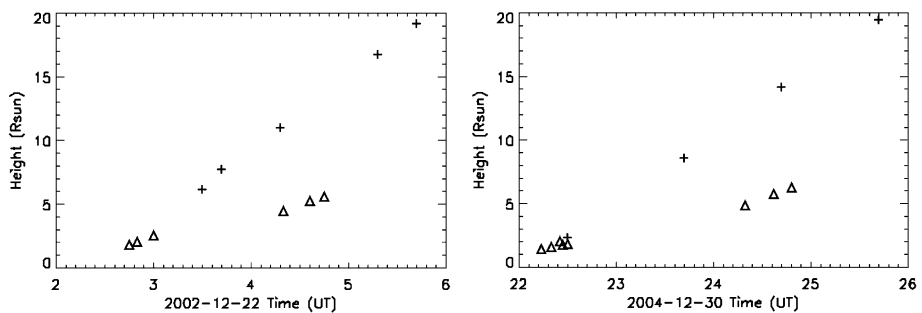
Figure 9 Height–time plots for the 22 December 2002 and the 30-31 December 2004 events. The heights of the CME leading fronts (crosses) can be compared with the heights of the metric and DH type II bursts (triangles).

coronagraph images in Figures 21 and 23 in the Appendix show streamers near the sides of the CMEs, and it is possible that the type II bursts were caused by shocks near the CME flanks, that were due to CME-streamer interaction at low heights.
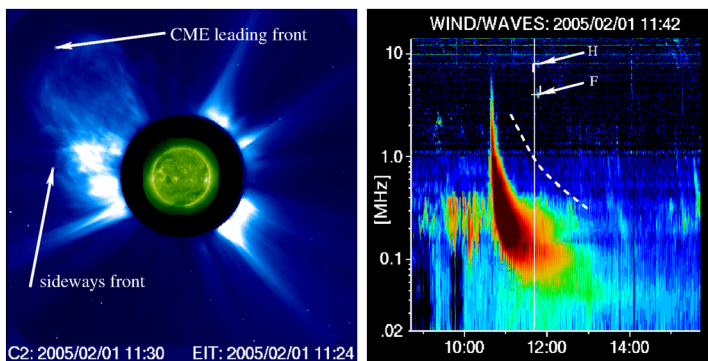
Figure 10 Event on 1 February 2005, source location at NE90b (on the far side). The leading front of the CME (white dashed line in the radio spectrum) is located 6.5 $R_\odot$ higher than the type II burst source. A lower, sideways propagating front is also visible near the south-east streamer in the LASCO C2 image (*left*).

Type III bursts were observed within the full frequency range in both events near the CME launch times, but later on the type III bursts showed 'cuts', i.e., the bursts were visible only at frequencies below the CME propagation heights, below ≈ 1 MHz. This suggests that either the type III electron beams were accelerated near the CME fronts or the CMEs blocked their visibility. Unfortunately these events occurred in the pre-STEREO era, so we cannot verify visibility toward other directions.

3.4. Event on 1 February 2005

In the 1 February 2005 event the CME originated from behind the east limb, and no X-ray flare was observed in the Earth view. The short, only five minute duration, DH type II burst showed both fundamental and harmonic emission (Figure 10). The leading front of the CME was faint and diffuse, and denser structures were located below it, at lower heights.

The coronal image processing (CORIMP) map (Figure 24 in the Appendix) also shows a lower front in the eastern flank of the CME (yellow lines). This lower front made a sudden south-westward movement in between the LASCO images at 11:30 UT and 11:54 UT, which matches with the short lifetime of the type II burst at 11:45 – 11:50 UT. It is most probable that the DH type II burst was a short-duration shock, created by the fast sideways movement within the CME.

4. Observations from Different Viewing Angles

In 12 cases the solar event could be observed from at least two different viewing angles, with the instruments onboard Wind, STEREO-A, and STEREO-B satellites. These events, with the DH type II burst start times and frequencies, are listed in Table 3 in the Appendix. In five events the radio emission start time and start frequency were different when observed from a different viewing angle. The start time delays were 5 min, 7 min, 8 min, 26 min, and 83 min, in the order of time delay. In one event the start time differed 2 min, but as the start frequency was the same in both, we concluded that there was no real delay in the type II start. We now describe the delayed events in more detail.

5 July 2012. The 5 min delay in the DH type II start looks to be due to band-splitting of the fundamental emission lane. The lower band-split lane start is observed at the same
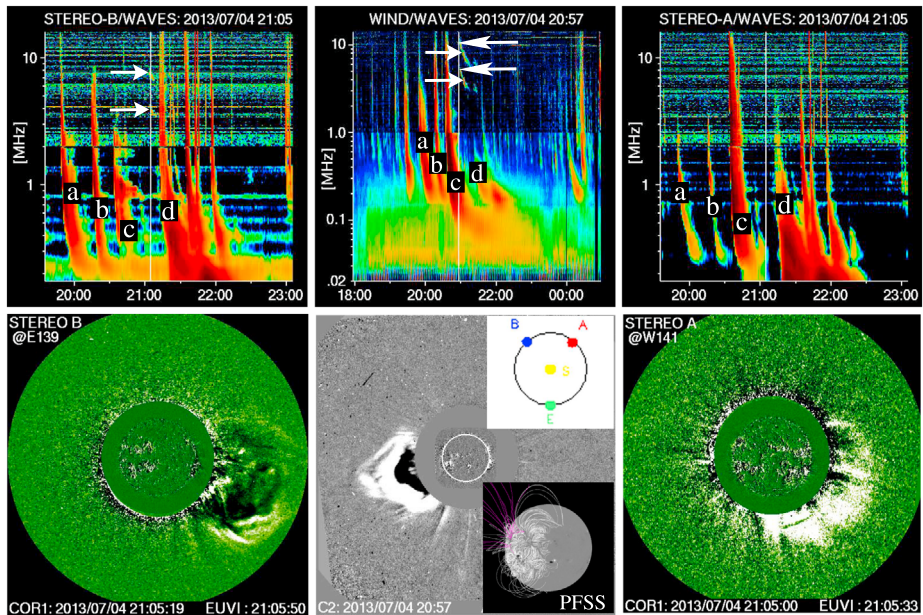
Figure 11 Comparison between STEREO-B, Wind, and STEREO-A observations on 4 July 2013. Longer arrows point to the first fundamental-harmonic structures observed by Wind and shorter arrows to the later emission structures observed also by STEREO-B. Type III bursts are labeled a–d, to compare their visibility with the different instruments. The burst source region was located at S14E62. Coronagraph and EUV difference images from the three different viewing angles are also shown, with the PFSS magnetic field extrapolation map (Earth view). Cartoon insert shows the positions of the three satellites, Wind in Earth view.

time with both Wind and STEREO-A instruments at 22:57 UT at ≈ 1.4 MHz, but STEREO-A records emission from the upper band-split lane earlier, at 22:52 UT at 2.2 MHz. The STEREO-A/WAVES dynamic spectrum also shows emission patches that can be interpreted as harmonic emission. Therefore the difference between the observations is most probably due to sensitivity, Wind/WAVES did not record the less intense emission from the upper split band. Moreover, a frequency drift from 2.2 MHz to 1.4 MHz within 5 min would require a burst driver speed of ≈ 3000 km s^{-1}, which also suggests that the emission structures did not belong to the same emission lane.

22 October 2012. The type II burst became visible 26 minutes earlier in the STEREO-B spectrum, compared to Wind and STEREO-A. By STEREO-B the burst started as a narrow lane at 01:24 UT at 1.4 MHz, but became much wider after 01:45 UT. The type II burst emission is very faint in the STEREO-A spectrum, but the start time is the same as in the Wind spectrum, at 01:50 UT. The beginning of the DH type II burst in the Wind spectrum is visible only partially below 1 MHz (Figure 30 in the Appendix), and therefore we conclude that this could also be a sensitivity issue between the Wind/WAVES RAD1 and RAD2 receivers.

4 July 2013. The time delay in the type II burst start was 8 min, as Wind observed the burst at 20:57 UT at 5 MHz and STEREO-B at 21:05 UT at 4 MHz (Figure 11). There were several type III bursts that preceded the type II burst, the closest-in-time are listed as a, b, c in the spectral plots. We note that the bursts b and c have a lower start frequency in the STEREO-B/WAVES spectrum, 8 MHz and 2.5 MHz, compared to the Wind/WAVES spectrum where the bursts are already visible at 14 MHz. This suggests that the emission of
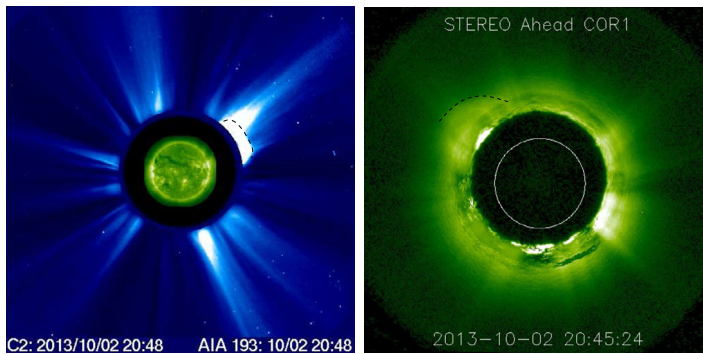
Figure 12 SOHO/LASCO C2 and SDO/AIA composite image (*left*) of the CME and its source region at N20W85 on 2 October 2013. The STEREO-A/COR1 coronagraph image (*right*) shows the same structure. The CME leading front is marked with a dashed line in both images. The LASCO C2 image shows a streamer that crosses the CME (in projection), but it is uncertain whether the streamer is located in front or behind of the CME bubble.

the type III bursts and the type II burst were occulted at low coronal heights in the STEREO-B view.

2 October 2013. STEREO-A observed the type II burst starting at 20:39 UT at 12 MHz and Wind later at 20:46 UT at 10 MHz. With the hybrid atmospheric density model a frequency drift from 12 to 10 MHz in 7 min would indicate a burst driver speed of ≈ 460 km s^{-1}. The CME speed at that time was ≈ 600 km s^{-1}, so the type II burst speed would be quite realistic.

We find there is a streamer visible in the SOHO/LASCO image, located across the (projected) CME loop (Figure 12). If the streamer location was such that it lay in between Wind and the type II shock, then STEREO-A would have been able to observe the type II directly, and Wind only through the streamer. Modeled streamer densities (Decraemer, Zhukov, and Van Doorsselaere, 2019) are very near to the type II density values at these heights.

It is therefore possible that the DH type II burst on 2 October 2013 became visible only when the type II burst emission frequency got above the plasma frequency of the streamer, when the streamer density and the critical plasma frequency decreased with height.

2 April 2014. This event showed the longest gap in the starting time of the type II burst, 83 min, as Wind recorded the burst start at 18:49 UT at 2.4 MHz and STEREO-B at 20:12 UT at 1.4 MHz. The type II burst was formed near a time when a new bright front appeared inside the main CME. The height difference between this new CME front and the type II burst was large only near the beginning of the radio burst (Figure 36, the Appendix), as after 19:40 UT the heights were a good match.

The curved structures in the Wind/WAVES spectrum, near the burst start, resemble those reported in Pohjolainen, Pomoell, and Vainio (2008). They found that the emission fragmentation was due to a shock passing through regions with highly variable densities, inside and outside high-density CME loops. Earlier launched CME loops on the shock propagation path would therefore be a good explanation for the emission curvature.

The type II burst was observed by STEREO-B only after 20:12 UT, i.e., the curved structures were not observed (Figure 13). STEREO-B was located 164 degrees back from Earth's orbit, almost directly on the opposite side of the Sun, so it should have had a good view to this new bright CME front. On the other hand, the earlier CME fragments were propagating toward north-east, i.e., toward STEREO-B, so occultation was possible.
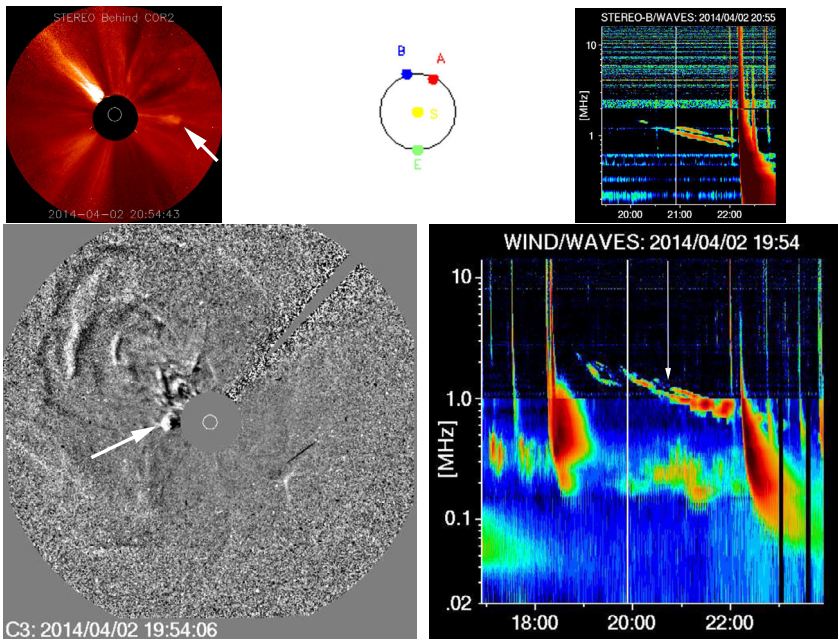
Figure 13 Wind, SOHO and STEREO-B observations on 2 April 2014. The active region associated with this event was located behind the north-eastern solar limb. Arrows point to the later CME structure (unlisted as a CME) that propagated inside the main CME. The fragments of the main CME are visible in the LASCO C3 difference image, north-east of the solar disc. STEREO-A observations are available only after 20:39 UT, and the recorded emission is similar to the STEREO-B observations. Wind/WAVES recorded the start of the type II burst 83 minutes before STEREO-B/WAVES.

5. Coronal Conditions for Type II Burst Formation

A large fraction of interplanetary shocks has been found to be radio quiet (Gopalswamy et al., 2010), and so even the appearance of a DH type II burst requires some specific coronal conditions. The simplest scenario would be that a shock is formed when the speed of a coronal transient exceeds the local magnetosonic speed, i.e., the Alfvén speed in the solar corona, and this leads to type II radio emission at some location along the shock front.

Figure 14 shows the calculated DH type II burst formation heights compared with the projected CME speeds. The dotted line in the plot shows how the Alfvén speed rises with distance from the Sun above an active region, and reaches a local maximum of $\approx 800 \text{ km s}^{-1}$ near $\approx 4 \text{ R}_\odot$ as in Kim et al. (2012). Even a higher value for the Alfvén speed, 1100 km s^{-1} at $3.5 \text{ R}_\odot$ as in Warmuth and Mann (2005), would not change the distribution of our events in most cases (below or above the Alfvén speed).

In six events the CME speed looks to be less than the assumed Alfvén speed. All six type II bursts were estimated to be due to CME bow shocks, as the type II heights matched well with the CME leading front heights, within the reasonable height calculation error. The height difference was $0.1 - 0.5 \text{ R}_\odot$ in the four events that were well below the Alfvén speed peak value, and 1.0 and $1.2 \text{ R}_\odot$ in the two events that were closer to the Alfvén speed value (the CME speeds in these two events were 700 and 720 km s^{-1}). The only F lane event among the six was a prominence eruption.

Figure 14 Type II burst formation height compared with the projected CME speed. The dotted line shows the local Alfvén speed, following the velocity curve presented in Kim et al. (2012). F and F+H lane bursts are plotted with different symbols and the three prominence eruption events are encircled.
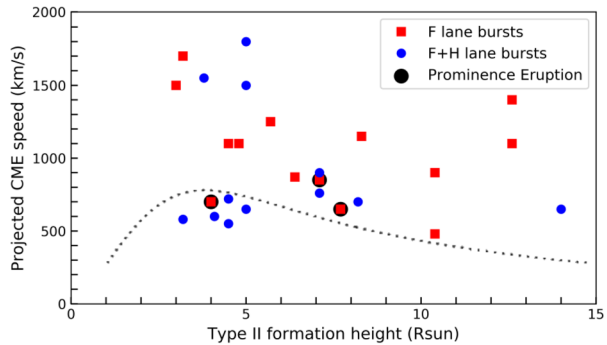
The four F+H lane type II bursts that had their CME speeds well below the modeled Alfvén speeds, had their source origin in similar locations on the solar disc, at longitudes E62, W63, W65, and W85. The CME speeds can be affected by projection effects in on-the-disc events, but a CME speed difference of $100-250$ km s^{-1} to the Alfvén speed cannot be explained with projection effects only. As these events were determined to be bow shock events, we conclude that the Alfvén speed had to be much lower in these coronal regions. This would be possible, for example, above some active regions and streamer regions (Evans et al., 2008). But for example Su et al. (2016) suggested that the generation of shocks, and type II bursts, may require larger values of compression ratio and Alfvén Mach number, rather than simply a higher speed of the disturbance.

Already Roberts (1959) reported to have observed fundamental and harmonic emission in 60% of all type II bursts. The intensity of the fundamental emission band has been observed to increase relative to the harmonic, as the burst evolves with heliocentric distance (Lengyel-Frey and Stone, 1989). The fundamental and harmonic frequencies are assumed to be products of three-wave interaction processes of beam-excited Langmuir waves. Langmuir waves would first have to scatter off sound waves at a sufficient rate to create a suitable population of counter-propagating Langmuir waves, and if this process was too slow, harmonic emission would not be able to attain intensities comparable to the fundamental plasma emission process (Ganse et al., 2012a).

Our correlation analysis showed that harmonic emission was present only in type II bursts that originated at longitudes larger than ±60 degrees. Our small sample of events, where six events originated inside the longitude range of E60 – W60 and showed one emission band, may contain selection effects. The overall ratio, 14 events with F band and 12 events with F+H band looks to be in agreement with previous studies.

6. Results and Discussion

We have analysed 26 well-separated, isolated DH type II radio bursts and compared their characteristics with active region, flare, and CME data. Association to metric type II emission and SEP (proton) events were also listed. First, we looked at the type II burst appearances and found bursts that showed a single emission lane (14 events, emission at the fundamental plasma frequency), and bursts with two lanes (12 events, fundamental and harmonic emission).

From the 26 events 8 had their source origin on the far side of the Sun, and 7 were limb events (longitudes 85 – 90 degrees east or west). Of the remaining 11 events, 6 were located

near the limb and 5 were located nearer to the disc center. No isolated DH type II bursts were observed inside the longitude range E30 – W40. At longitudes E30 – 50 and W40 – 50 all the isolated type II bursts were single lane bursts (no harmonic emission).

The fastest CMEs associated with the DH type II bursts were observed in events that originated at or behind the solar limb. This is understandable, as height measurements of on-the-disc CMEs may suffer from projection effects. A similar result was obtained by Vasanth and Umapathy (2013). The associated CMEs had variable widths, in the range of 40 – 230 degrees near the time of the DH type II burst start. The narrowest CMEs were in events that occurred at or behind the solar limb. The closer to the disc center the event originated, the larger the CME angular width. The largest angular widths were associated with low-frequency start of emission (i.e., high formation height of the type II burst), although low-frequency onset of emission occurred also in events where the CME had very narrow width.

Of the 26 events, 16 were found to have a good match between the DH type II burst height and the CME leading front height, within the possible $\pm 2\,\mathrm{R}_\odot$ error. In other five events we could also make a match to the CME leading front if the whole radio emission lane and later times along the type II lane were considered for the height calculation. These type II bursts could be due to CME bow shocks, located near the CME nose. We note that in several cases the radio burst height was closer to the bright front structure of the CME, and not to the diffuse region above it (if it existed) that is often taken as the CME height. Shock regions and CME structures are discussed, for example, in Kwon and Vourlidas (2018), Song et al. (2019), and Mei et al. (2020), and the references therein.

Only five events showed a large height difference between the DH type II shock and the CME leading front, and these events were analysed in detail. For the DH type II burst that was located much higher than the CME leading front we found a possible explanation from two earlier CMEs that had comparable heights with the type II burst. This event was observed also with STEREO-A/WAVES, and the spectral features there suggest that the type II-like bursts could also have been radio enhancements along type III burst lanes, formed by electron beams passing through the earlier-launched CME material.

For the four DH type II bursts that showed heights much lower than the CME leading front we found the following explanations. The two DH type II bursts with source origins at longitudes W42 and E46 and emission only at the fundamental frequency, a CME flank shock looks to be the most probable explanation. In one event a later-launched CME structure, inside the main CME, was visible and the curvature of the type II lane matched with the height evolution of the later CME. For one event, a fast sideways movement of a lower CME structure, creating a short-duration shock, may have been the cause for the type II burst.

Our sample of isolated DH type bursts, where most bursts look to be due to shocks near the CME leading front, contradicts earlier findings. DH type II bursts, using for example radio triangulation method, have in most studies been found to be located near the CME flank regions, and only in few cases have been located close to the CME nose; see Jebaraj et al. (2020) and the references therein. A statistical study of 153 interplanetary type II radio bursts observed by the two STEREO spacecraft in 2008 – 2014 (Krupar et al., 2019) also suggested that interplanetary type II bursts are more likely to have a source region situated closer to the CME flanks than the CME leading edge. The radio bursts located near the CME flanks have also been noted to be enhanced by shock-streamer interaction (Shen et al., 2013).

The results of Kahler, Ling, and Gopalswamy (2019) suggested that fast and narrow CMEs can create mostly bow shocks, and fast and wide CMEs predominately expansion shocks. Also Vourlidas and Ontiveros (2009) have suggested that the bow shock morphology is associated almost exclusively with narrow CMEs. Kahler, Ling, and Gopalswamy (2019)

further concluded that no CMEs with widths less than 60° are associated with metric type II bursts. Our study confirms this finding, but we point out that CMEs with widths less than 60° can still be associated with DH type II bursts.

Of our 26 DH type II burst events, 10 were associated with earlier metric type II bursts. All 10 metric bursts died out before reaching the DH instrumental limit of 16/14 MHz, and the later-appearing DH bursts were isolated. We note that the metric type II bursts were formed only with the fastest CMEs, with a CME velocity range of $1100 – 1800$ km s^{-1}. It has been suggested earlier that metric type II radio bursts are formed by a distinct coronal shock and only produce radio emission in the low corona, see, e.g., Reiner et al. (2000) and Magara et al. (2000), but opposite arguments have also been made; see Gopalswamy et al. (1999) and the references therein.

In three of our events the start time of the DH type II burst matched well with the solar energetic particle (SEP) release time for protons in the $55 – 80$ MeV range. In two SEP-associated events earlier metric type II emission was observed, but 21 of the isolated DH type II bursts were not associated with listed proton events.

Comparison between the Wind and STEREO observations, available for 12 events, showed that the DH type II burst start was not always observed toward all directions. There was a delay in the starting times in five events. In two events only Wind recorded the DH type II burst, and both were eruptive prominences with source longitude at E30. Of the five events that showed time delays, two seemed to suffer from sensitivity issues in the radio spectral data. Less intense emission near the DH type II start could therefore go unnoticed. In the other three events, occultation by a dense streamer or earlier-launched CME fragments looked possible. Radio emission from the DH type II burst would become visible only when the type II burst frequency exceeds the plasma frequency of the occulting structure, i.e., when the density of the occulting structure is less than in the type II shock region.

In Section 5 we discussed the required conditions in the corona for the development of a shock wave. It is well known that not all coronal shocks produce DH type II bursts. In most of our analysed events, the CME speed looked to be well above the local Alfvén speed, and therefore type II emission would be possible. Some of the DH type II bursts had very short duration, which indicates that either the emission ended or it became unobservable (invisible). In general, the DH type II burst duration was found to depend on the type II burst start frequency, i.e., the lower the start frequency the longer the duration.

Type II bursts have a quite narrow emission band (narrow range of densities), and therefore the emission region cannot be spread out along a large area of the (curved) shock front. The small-scale type II emission region is thus expected to have special properties, setting it apart from the rest of the shock (Ganse et al., 2012b). A specific local region would also provide the conditions for the enhancement of emission near the plasma frequency harmonics (Annenkov, Volchok, and Timofeev, 2020).

7. Conclusions

We conclude that isolated DH type II bursts can be narrow-band or wide-band, can have short or long duration, and can show only fundamental or both fundamental and harmonic emission. The bursts typically have their source origin some distance away from the central meridian, at longitudes $30 – 90$ degrees east or west, but only some of the bursts originate from the far side of the Sun.

Almost all of the analysed 26 isolated DH type II bursts could be associated with a shock near the leading front of the main CME. In only two events a shock near the CME flanks

was estimated to be the cause of the DH type II burst, and in three events the radio bursts could be explained by earlier or later CME structures. Our analysis suggests that for the majority of isolated DH type II bursts a CME bow shock is more probable than a CME flank shock.

We also analysed the radio spectral data from different viewing angles in 12 events, provided by the STEREO and Wind spacecraft observations. We compared the spectral features of the DH type II bursts, and their timing. In five events a time delay in the DH type II start was evident, and only one of the five was a far side event. In three events occultation by dense matter between the source and the observer could have been the cause for the delay in the emission onset, and in two events spectral sensitivity could have affected the observed starting time.

Why do some DH type II bursts appear isolated, without other radio emission signatures, and why do many of them disappear from the spectrum as suddenly as they appear? Our findings suggest that isolated DH type II bursts could be a special subgroup within DH type II bursts, where the radio emission requires particular coronal conditions to form, and the bursts can die out rapidly if these conditions change.

Appendix: Event Images

For each event we show a coronagraph-EUV difference image (SOHO/LASCO - SOHO/ EIT), a Wind/WAVES radio dynamic spectrum that shows the DH type II burst, and a CORIMP map or a coronagraph image (LASCO or STEREO) that shows the streamer locations. In the radio dynamic spectra the white vertical lines indicate the time of the coronagraph image, and white arrows point to the type II burst structures (one arrow for a single F lane event and two arrows labeled F and H if a harmonic lane is visible). The white dashed lines in the radio spectra indicate CME heights converted to frequencies, with the hybrid plasma density model by Vrsnak, Magdalenic, and Zlobec (2004). The LASCO C2-C3 image from the CORIMP catalogue (or the coronagraph image) is from a time close to the type II start or during the type II burst. In the CORIMP images the yellow lines detail the detected CME structure, and the red points correspond to the outer features that are used for tracking the CME heights (see details in the CORIMP catalogue at http://alshamess.ifa.hawaii.edu/ CORIMP/). EP stands for eruptive prominence.
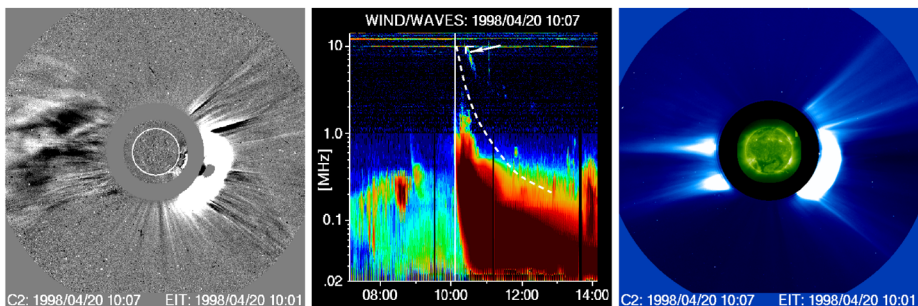
Figure 15 20 April 1998, source location S22W90.
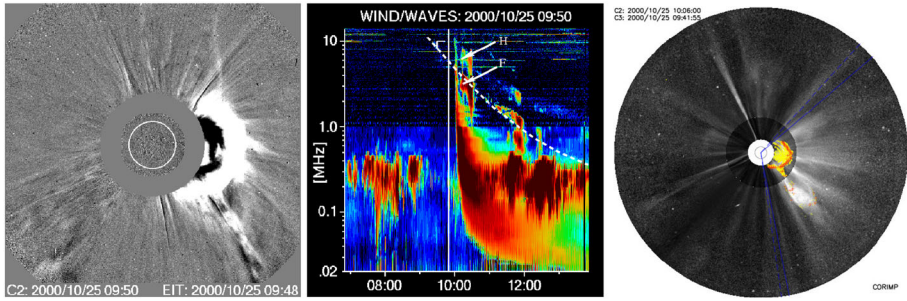
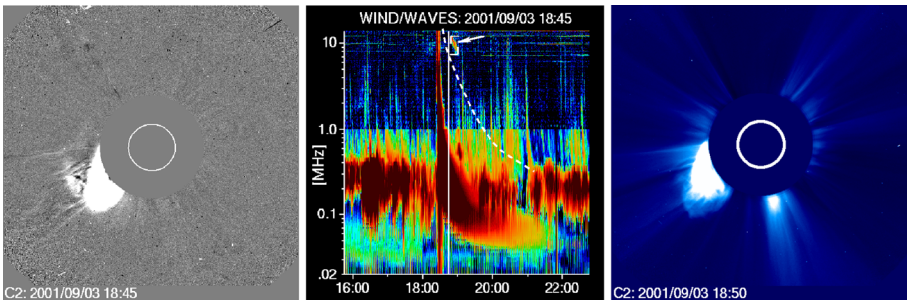**Figure 16**	25 October 2000, source location N09W63.
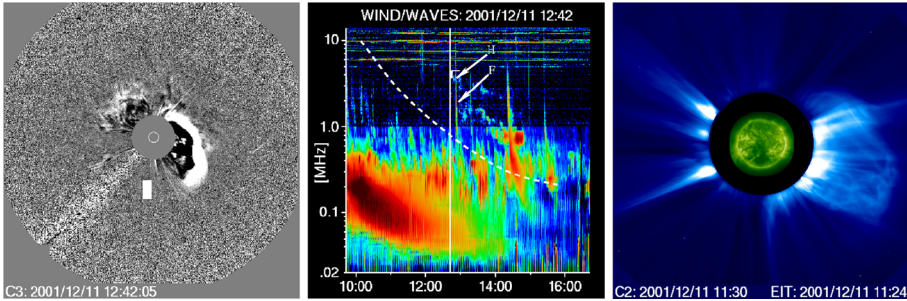

Figure 17	3 September 2001, source location S23E90.

Figure 18	11 December 2001, source location SW90b. The DH type II burst was estimated to be located ≈6 $R_\odot$ lower than the CME leading front, and this event is analysed in more detail in Section 3.2.

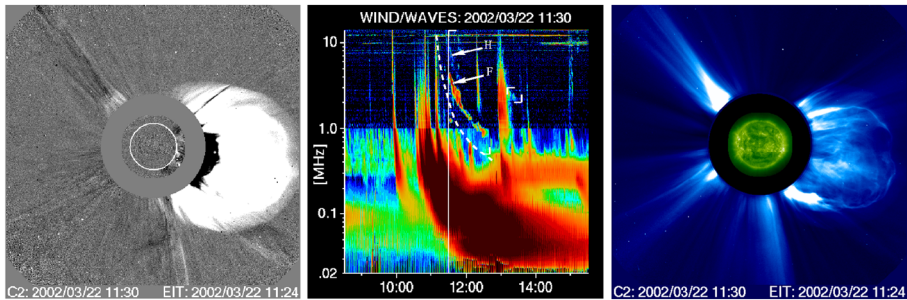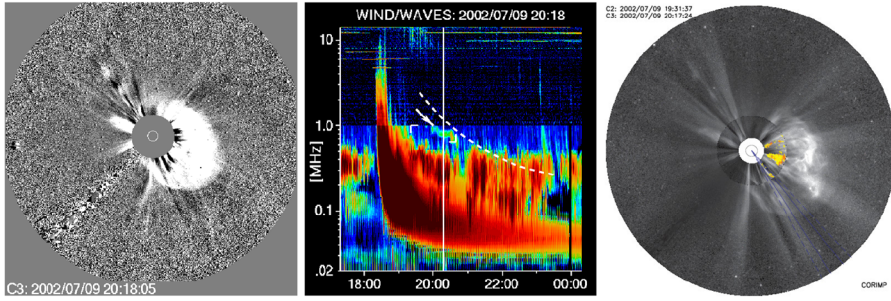**Figure 19**	22 March 2002, source location S09W90.
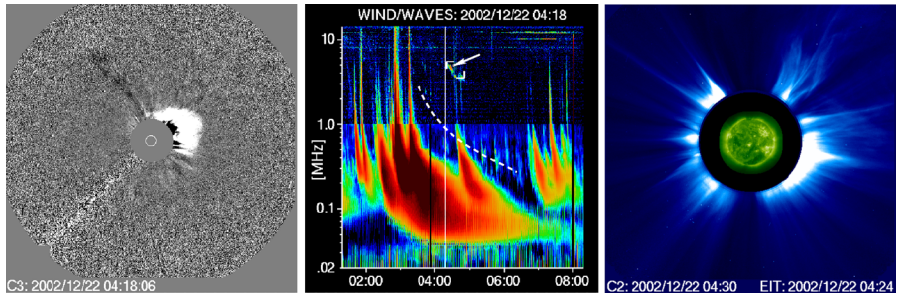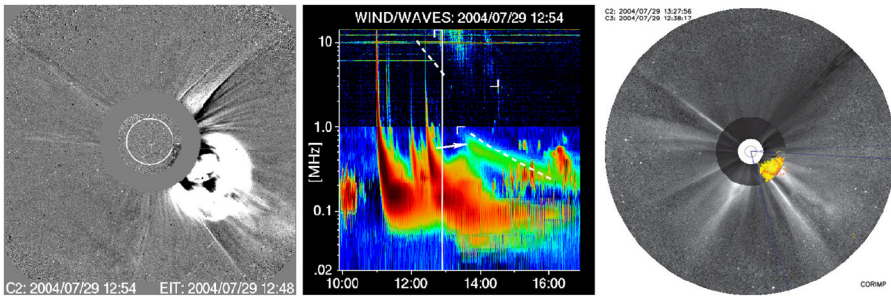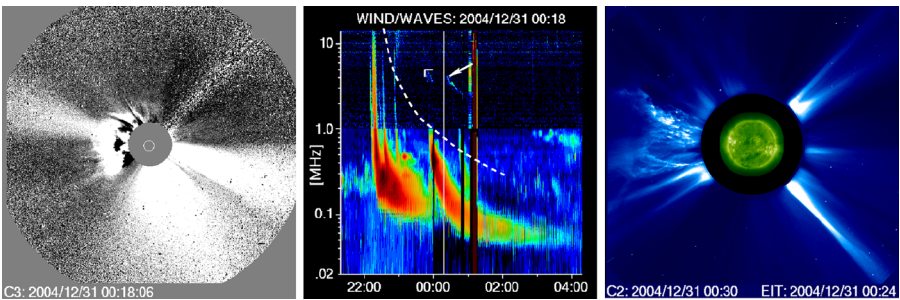
Figure 20 9 July 2002, source location W90b.

Figure 21 22 December 2002, source location N23W42. The DH type II burst source was estimated to be located ≈7 R$_\odot$ lower than the CME leading front, and this event is analysed in more detail in Section 3.3.

Figure 22 29 July 2004, source location N00W90.

Figure 23 31 December 2004, source location N04E46. The DH type II burst source was estimated to be located ≈7 R$_\odot$ lower than the CME leading front, and this event is analysed in more detail in Section 3.3.
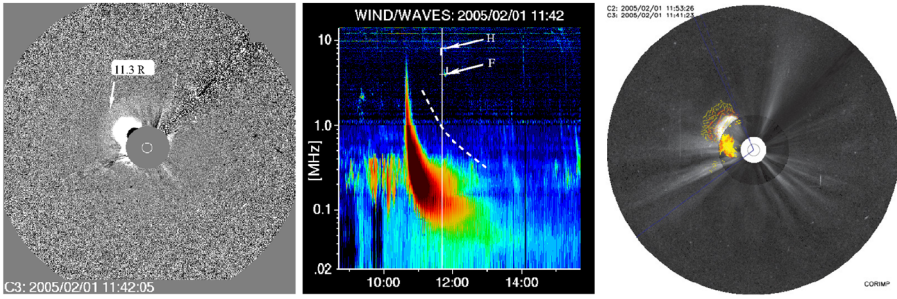
Figure 24 1 February 2005, source location NE90b. The DH type II burst was estimated to be located ≈ 6 $R_\odot$ lower than the CME leading front, and this event is analysed in more detail in Section 3.4.
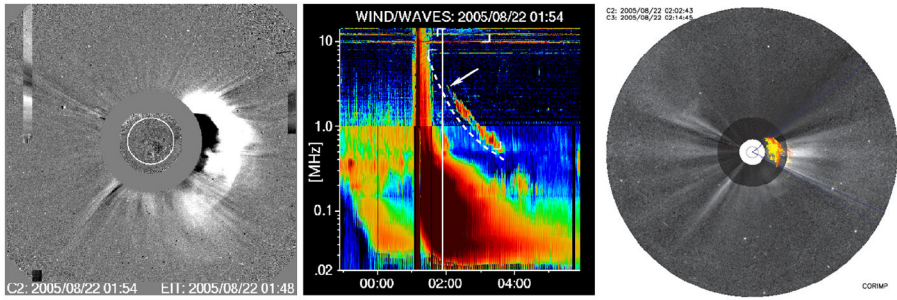
Figure 25   22 August 2005, source location S11W54.
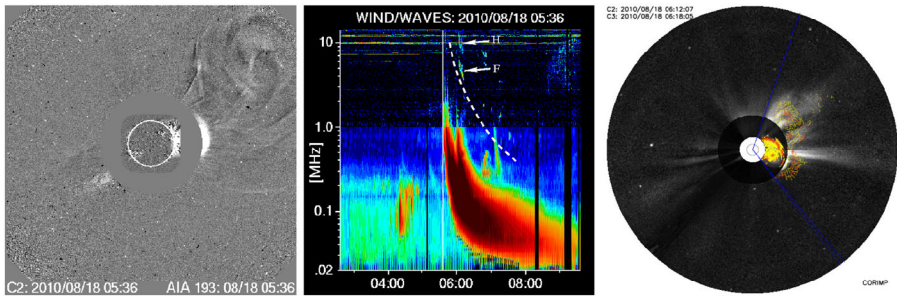
Figure 26   18 August 2010, source location N18W88.
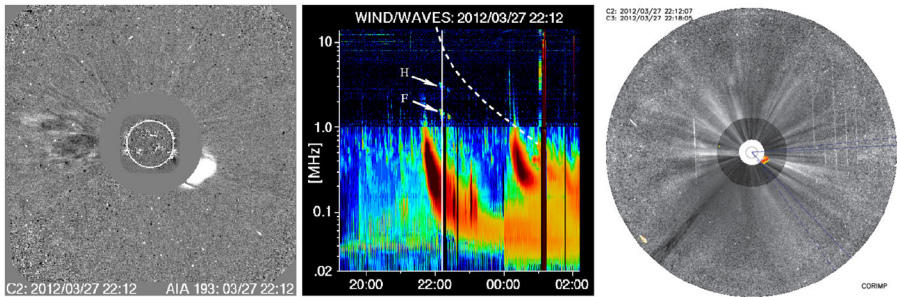
Figure 27   27 March 2012, source location SW90b. The leading front of the CME was located ≈ 5 $R_\odot$ lower than the DH type II burst source, and this event is analysed in more detail in Section 3.1.
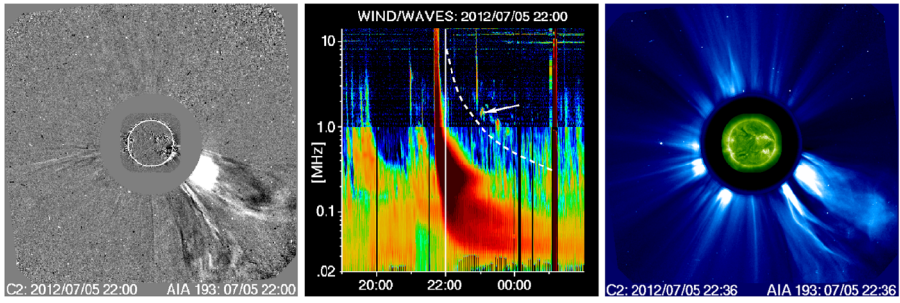
Figure 28 5 July 2012, source location S12W46. This event is discussed in more detail in Section 4 (delay in DH type II burst start, STEREO observations).
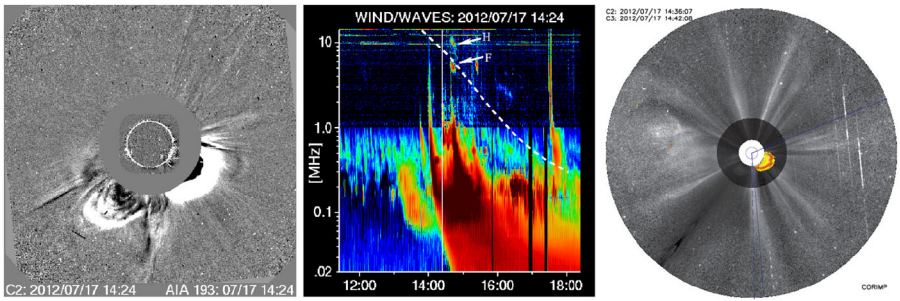

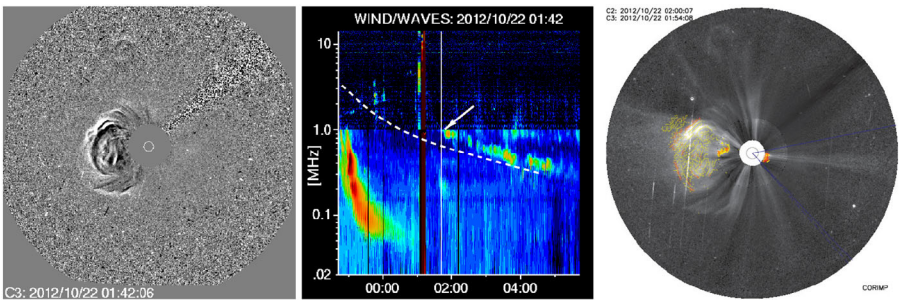**Figure 29** 17 July 2012, source location S28W65.

Figure 30 22 October 2012, source location S10E76. This event is discussed in more detail in Section 4 (delay in DH type II burst start, STEREO observations).
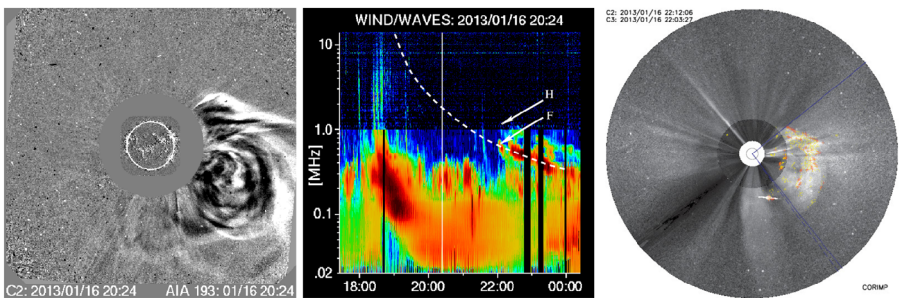

Figure 31 16 January 2013, source location S33W64.
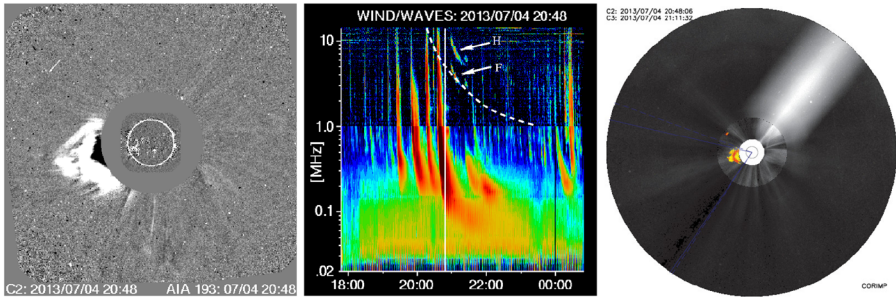
Figure 32 4 July 2013, source location S14E62. This event is discussed in more detail in Section 4 (delay in DH type II burst start, STEREO observations).
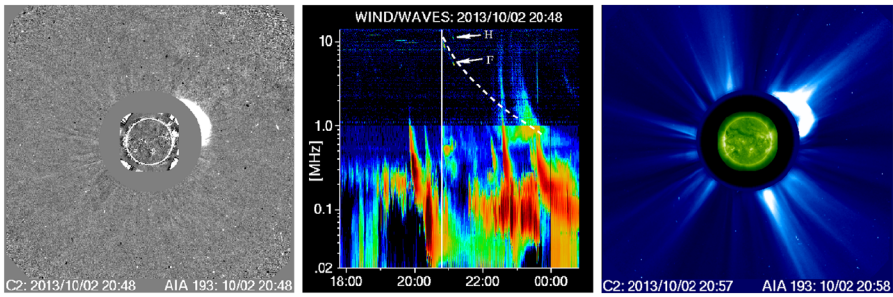

Figure 33 2 October 2013, source location N20W85. This event is discussed in more detail in Section 4 (delay in DH type II burst start, STEREO observations).
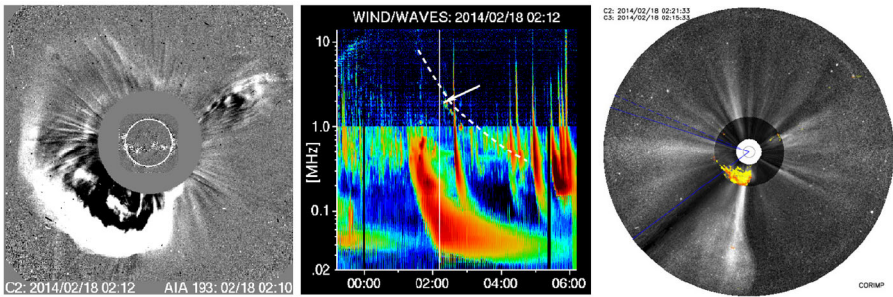

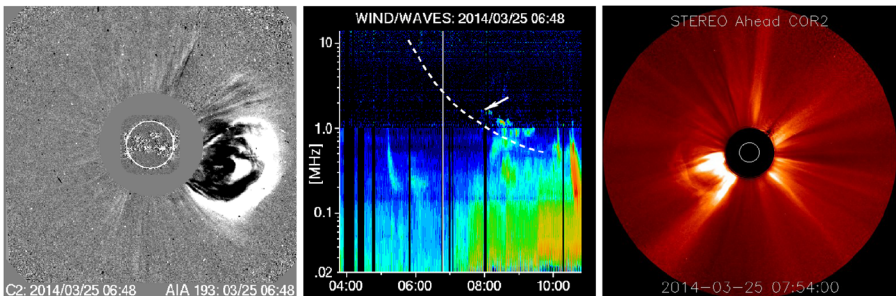**Figure 34** 18 February 2014, source location SE30 (EP).

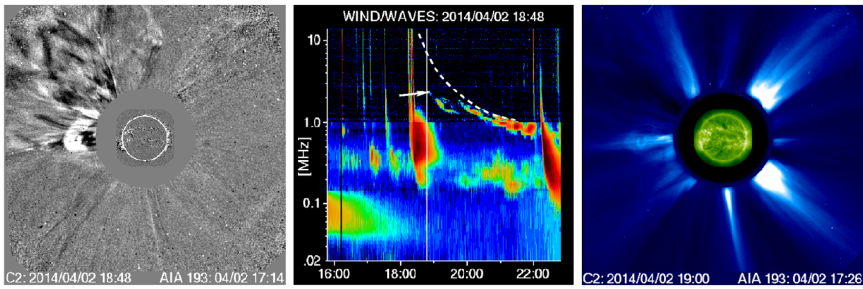**Figure 35** 25 March 2014, source location S23W90b (EP).

Figure 36 2 April 2014, source location NE90b. The unlisted CME front was propagating inside an earlier CME. This later front propagation is indicated with the dashed line in the dynamic spectrum. The earlier, listed CME front was last observed at height 28 $R_\odot$ at 16:54 UT, which corresponds to $\approx$0.2 MHz frequency. This event is discussed in more detail in Section 4 (delay in DH type II burst start, STEREO observations).
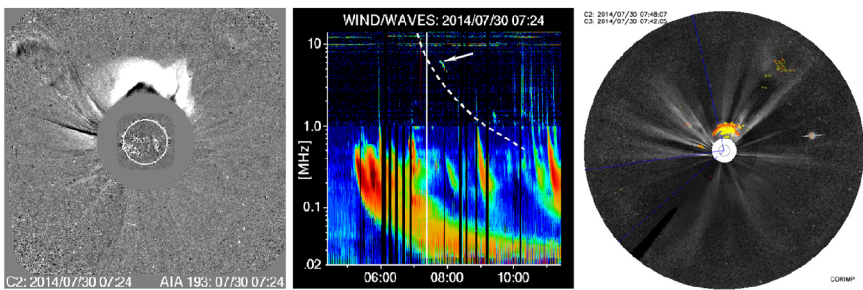

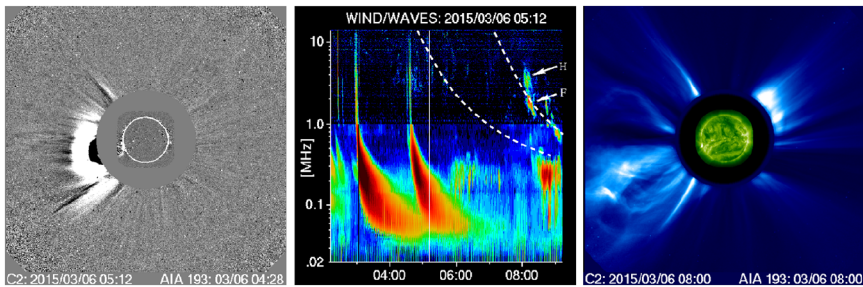**Figure 37** 30 July 2014, source location N10E30 (EP).

Figure 38 6 March 2015, source location S20E87. The CME was propagating in the wake of an earlier CME, and both CMEs are listed in the CME Catalog.
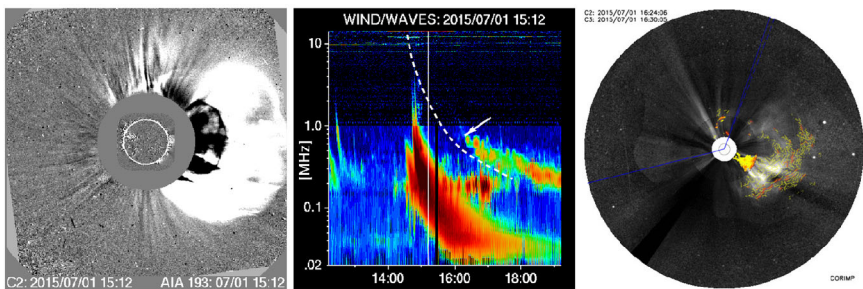

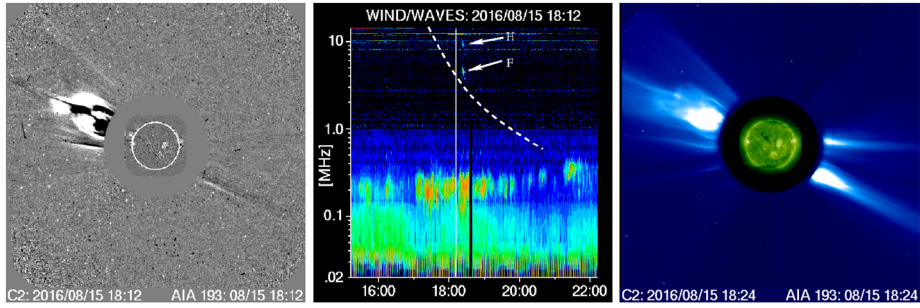**Figure 39** 1 July 2015, source location W90b.

Figure 40   15 August 2016, source location E90b.

Table 1   Selected DH type II bursts, a total of 26 events. Flare/prominence location, CME type (H indicates halo, PH partial halo, and - not halo), and comparison between the type II height and the simultaneous CME height (Δh) are listed.

Date yyyy-mm-dd	Type II start UT	Dur. min.	F-lane MHz	F-height R$_\odot$	CME height R$_\odot$	Δh CME-F R$_\odot$	Flare/prom. loc.	CME type
1998-04-20	10:25	10	10	3.2	5.0	1.8	S22W90	PH
2000-10-25	10:00	120+	4	5.0	4.5	−0.5	N09W63	H
2001-09-03	18:48	12	12	3.0	4.1	1.1	S23E90	PH
2001-12-11	12:45	120	2	7.1	13.0	5.9	SW90b	PH
2002-03-22	11:30	70	4	5.0	7.0	2.0	S09W90	H
2002-07-09	19:46	54	1	10.4	7.3	−3.1	W90b	H
2002-12-22	04:20	30	5	4.5	11.2	6.7	N23W42	PH
2004-07-29	13:30	300+	0.7	12.6	10.0	−2.6	N00W90	H
2004-12-31	00:19	29	4.2	4.8	12.0	7.2	N04E46	H
2005-02-01	11:45	5	4	5.0	11.5	6.5	NE90b	H
2005-08-22	02:00	95	3	5.7	7.0	1.3	S11W54	H
2010-08-18	06:01	11	7	3.8	4.8	1.0	N18W88	PH
2012-03-27	22:10	20	1.5	8.2	3.0	−5.2	SW90b	-
2012-07-05	22:57	60	1.4	8.3	9.0	0.7	S12W46	-
2012-07-17	14:40	8	6	4.1	4.0	−0.1	S28W65	PH
2012-10-22	01:50	500+	1	10.4	13.3	2.9	S10E76	PH
2013-01-16	22:00	180	0.6	14.0	13.5	−0.5	S33W64	PH
2013-07-04	20:57	18	5	4.5	4.9	0.4	S14E62	PH
2013-10-02	20:46	24	10	3.2	2.8	−0.4	N20W85	PH
2014-02-18	02:16	35	2	7.1	6.2	−0.9	SE30	H
2014-03-25	07:52	83	1.7	7.7	9.6	1.9	S23W90b	PH
2014-04-02	18:49	230+	2.4	6.4	3.8	−2.6	NE90b	H
2014-07-30	07:44	16	6.3	4.0	5.2	1.2	N10E30	PH
2015-03-06	08:10	140	2.0	7.1	7.2	0.1	S20E87	PH
2015-07-01	16:22	260	0.7	12.6	16.0	3.4	W90b	H
2016-08-15	18:21	7	5.0	4.5	5.5	1.0	E90b	-

Table 2 Selected DH type II bursts and associated events.

Date yyyy-mm-dd	AR	GOES class	CME first obs. UT	CME speed[1] km s^{-1}	CME width[2] deg	Metric type II	DH band $\Delta f/f$	DH lane
1998-04-20	8194	M1.4	10:07	1700 ac.	120	yes	0.04	F
2000-10-25	9199	C4.0	08:26	650 ac.	120	-	0.30	F+H
2001-09-03	9607	M2.5	18:35	1500 de.	70	yes	0.06	F
2001-12-11	-	-	09:54[3]	900 ac.	120	-	0.25	F+H
2002-03-22	9866	M1.6	11:06	1800 de.	110	yes	0.12	F+H
2002-07-09	-	-	19:31	900 de.	200	-	0.20	F
2002-12-22	10223	M1.1	03:30	1100 de.	120	yes	0.12	F
2004-07-29	10652	C2.1	12:06	1100 ac.	100	-	0.36	F
2004-12-31	10715	M4.2	22:30	1100 co.	130	yes	0.07	F
2005-02-01	-	-	11:06	1500 de.	100	yes	0.10	F+H
2005-08-22	10798	M2.6	01:31	1250 de.	180	yes	0.10	F
2010-08-18	11099	C4.5	05:48	1550 de.	90	yes	0.14	F+H
2012-03-27	-	-	22:00	700 co.	45	-	0.20	F+H
2012-07-05	11515	M1.6	22:00	1150 de.	60	yes	0.21	F
2012-07-17	11520	C9.9	13:48	600 ac.	80	-	0.18	F+H
2012-10-22	11598	M1.3	20:57	480 ac.	180	-	0.20	F
2013-01-16	11650	C2.2	19:00	650 de.	180	-	0.33	F+H
2013-07-04	11787	C6.8	20:12	550 de.	85	-	0.10	F+H
2013-10-02	11850	C1.2	20:36	580 ac.	70	-	0.05	F+H
2014-02-18	EP	-	01:25	850 de.	230	-	0.10	F
2014-03-25	EP	-	05:36	650 ac.	80	-	0.09	F
2014-04-02	-	-	13:36[4]	870 de.	50	-	0.12	F
2014-07-30	EP?	-	07:00	700 co.	100	-	0.05	F
2015-03-06	12297	M1.5	07:12[5]	760 ac.	120	-	0.30	F+H
2015-07-01	-	-	14:36	1400 de.	200	yes	0.21	F
2016-08-15	-	-	17:24	720 de.	40	-	0.10	F+H

[1]CME speed at the time of DH type II burst start, from second order fit, with acceleration/deceleration/constant speed information (CDAW CME Catalog).

[2]CME angular width at the time of type II burst start.

[3]Later CME front observed at 11:30 UT, inside the listed CME, speed 500 km s^{-1} and accelerating.

[4]Long-duration X-ray flare, bright propagating CME front appears at 18:36 within the listed CME, height and speed are for the new feature.

[5]Propagating in the wake of an earlier CME.

Table 3 DH type II bursts observed with Wind and STEREO (total of 12 events).

Date	STEREO-B UT/MHz	Wind UT/MHz	STEREO-A UT/MHz	Source	Comment
2010-08-18	-	06:01/7.0	06:01/7.0	N18W88	No delay
2012-03-27	-	22:06/1.5	22:06/1.5	SW90b	No delay
2012-07-05	-	22:57/1.4	22:52/2.2	S12W46	A first, 5 m
2012-07-17	-	14:40/6.0	14:40/6.0	S28W65	No delay
2012-10-22	01:24/1.4	01:50/1.0	01:50/0.9	S10E76	B first, 26 m
2013-07-04	21:05/4.0	20:57/5.0	-	S14E62	Wind first, 8 m
2013-10-02	-	20:46/10.0	20:39/12.0	N20W85	A first, 7 m
2014-02-18	-	02:16/2.0	-	SE30	Wind only, EP
2014-03-25	07:54/1.7	07:52/1.7	07:54/1.7	S23W90b	No delay, EP
2014-04-02	20:12/1.4	18:49/2.4	no observ.	NE90b	Wind first, 83 m
2014-07-30	-	07:44/6.3	-	N10E30	Wind only, EP?
2016-08-15	no observ.	18:21/5.0	18:21/5.0	E90b	No delay

Declarations

Disclosure of Potential Conflicts of Interest   The authors declare that they have no conflicts of interest.

References

Aguilar-Rodriguez, E., Gopalswamy, N., MacDowall, R., Yashiro, S., Kaiser, M.L.: 2005, A universal characteristic of type II radio bursts. *J. Geophys. Res.* **110**, A12S08. DOI.

Annenkov, V.V., Volchok, E.P., Timofeev, I.V.: 2020, Electromagnetic emission produced by three-wave interactions in a plasma with continuously injected counterstreaming electron beams. *Astrophys. J.* **904**, 88. DOI.

Bastian, T.S.: 2007, Synchrotron radio emission from a fast halo coronal mass ejection. *Astrophys. J.* **665**, 805. DOI.

Cane, H., Sheeley, N.R., Howard, R.A.: 1987, Energetic interplanetary shocks, radio emission, and coronal mass ejections. *J. Geophys. Res.* **92**, 9869. DOI.

Decraemer, B., Zhukov, A.N., Van Doorsselaere, T.: 2019, Three-dimensional density structure of a solar coronal streamer observed by SOHO/LASCO and STEREO/COR2 in quadrature. *Astrophys. J.* **883**, 152. DOI.

Evans, R.M., Opher, M., Manchester, W.B. IV, Gombosi, T.I.: 2008, Alfvén profile in the lower corona: Implications for shock formation. *Astrophys. J.* **687**, 1355. DOI.

Ganse, U., Kilian, P., Spanier, F., Vainio, R.: 2012a, Nonlinear wave interactions as emission process of type II radio bursts. *Astrophys. J.* **751**, 145. DOI.

Ganse, U., Kilian, P., Vainio, R., Spanier, F.: 2012b, Emission of type II radio bursts - Single-beam versus two-beam scenario. *Solar Phys.* **280**, 551. DOI.

Gopalswamy, N.: 2000, Type II solar radio bursts. In: *Radio Astronomy at Long Wavelengths*, *AGU Geophys. Monograph Ser.* **119**, 123. https://agupubs.onlinelibrary.wiley.com/doi/10.1029/GM119p0123.

Gopalswamy, N., Kaiser, M.L., Lepping, R.P., Kahler, S.W., Ogilvie, K., Berdichevsky, D., Kondo, T., Isobe, T., Akioka, M.: 1999, Reply [to "Comment on "Origin of coronal and interplanetary shocks: A new look with Wind spacecraft data" by N. Gopalswamy et al."]. *J. Geophys. Res.* **104**, 4749. DOI.

Gopalswamy, N., Yashiro, S., Kaiser, M.L., Howard, R.A., Bougeret, J.-L.: 2001, Characteristics of coronal mass ejections associated with long-wavelength type II radio bursts. *J. Geophys. Res.* **106**, 29219. DOI.

Gopalswamy, N., Yashiro, S., Michalek, G., Kaiser, M.L., Howard, R.A., Bougeret, J.L.: 2002, Statistical properties of radio-rich coronal mass ejections. In: Wang, H., Xu, R. (eds.) *Solar-Terrestrial Magnetic Activity and Space Environment, COSPAR Colloq. Ser.* **14**, 169. DOI.

Gopalswamy, N., Xie, H., Mäkelä, P., Akiyama, S., Yashiro, S., Kaiser, M.L., Howard, R.A., Bougeret, J.-L.: 2010, Interplanetary shocks lacking type II radio bursts. *Astrophys. J.* **710**, 1111. DOI.

Iwai, K., Yashiro, S., Nitta, N.V., Kubo, Y.: 2020, Spectral structures of type II solar radio bursts and solar energetic particles. *Astrophys. J.* **888**, 50. DOI.

Jebaraj, I.C., Magdalenic, J., Podladchikova, T., Scolini, C., Pomoell, J., Veronig, A., Dissauer, K., Krupar, V., Kilpua, E., Poedts, S.: 2020, Using radio triangulation to understand the origin of two subsequent type II radio bursts. *Astron. Astrophys.* **639**, A56. DOI.

Kahler, S.W., Ling, A.G., Gopalswamy, N.: 2019, Are solar energetic particle events and type II bursts associated with fast and narrow coronal mass ejections? *Solar Phys.* **294**, 134. DOI.

Kim, R.-S., Gopalswamy, N., Moon, Y.-J., Cho, K.-S., Yashiro, S.: 2012, *Astrophys. J.* **746**, 118. DOI.

Krupar, V., Magdalenic, J., Eastwood, J.P., Gopalswamy, N., Kruparova, O., Szabo, A., Nemec, F.: 2019, Statistical survey of coronal mass ejections and interplanetary type II bursts. *Astrophys. J.* **882**, 92. DOI.

Kwon, R-Y., Vourlidas, A.: 2018, The density compression ratio of shock fronts associated with coronal mass ejections. *J. Space Weather Space Clim.* **8**, A08. DOI.

Lee, J.-O., Moon, Y.-J., Lee, J.-Y., Kim, R.-S., Cho, K.-S.: 2017, Which bow shock theory, gasdynamic or magnetohydrodynamic, better explains CME stand-off distance ratios from LASCO-C2 observations? *Astrophys. J.* **838**, 70. DOI.

Lengyel-Frey, D., Stone, R.G.: 1989, Characteristics of interplanetary type II radio emission and the relationship to shock and plasma properties. *J. Geophys. Res.* **94**, 159. DOI.

Lengyel-Frey, D., Stone, R.G., Bougeret, J.L.: 1985, Fundamental and harmonic emission in interplanetary type II radio bursts. *Astron. Astrophys.* **151**, 215.

Magara, T., Chen, P., Shibata, K., Yokoyama, T.: 2000, A unified model of coronal mass ejection-related type II radio bursts. *Astrophys. J.* **538**, L175. DOI.

Mann, G., Klassen, A., Aurass, H., Classen, H.-T.: 2003, Formation and development of shock waves in the solar corona and the near-Sun interplanetary space. *Astron. Astrophys.* **400**, 329. DOI.

Mei, Z.X., Keppens, R., Cai, Q.W., Ye, J., Li, Y., Xie, X.Y., Lin, J.: 2020, The triple-layered leading edge of solar coronal mass ejections. *Astrophys. J. Lett.* **898**, L21. DOI.

Mittal, N., Verma, V.K.: 2017, Relationship of decametric-hectometric type II radio burst, coronal mass ejections and solar flare observed during 1997–2014. *New Astron.* **50**, 60. DOI.

Paassilta, M., Raukunen, O., Vainio, R., Valtonen, E., Papaioannou, A., Siipola, R., Riihonen, E., Dierckxsens, M., Crosby, N., Malandraki, O., Heber, B., Klein, K.-L.: 2017, Catalogue of 55-80 MeV solar proton events extending through solar cycles 23 and 24. *J. Space Weather Space Clim.* **7**, A14. DOI.

Pappa Kalaivani, P., Umapathy, S., Shanmugaraju, A., Prakash, O.: 2010, Characteristics of coronal mass ejection associated with DH type II radio bursts (All and Limb events). *Astrophys. Space Sci.* **330**, 237. DOI.

Payne-Scott, R., Yabsley, D.E., Bolton, J.G.: 1947, Relative times of arrival of bursts of solar noise on different radio frequencies. *Nature* **160**, 256.

Pick, M., Vilmer, N.: 2008, Sixty-five years of solar radioastronomy: Flares, coronal mass ejections and Sun-Earth connection. *Astron. Astrophys. Rev.* **16**, 1. DOI.

Pohjolainen, S., Allawi, H., Valtonen, E.: 2013, Origin of wide-band IP type II bursts. *Astron. Astrophys.* **558**, A7. DOI.

Pohjolainen, S., Pomoell, J., Vainio, R.: 2008, CME liftoff with high-frequency fragmented type II burst emission. *Astron. Astrophys.* **490**, 357. DOI.

Pohjolainen, S., van Driel-Gesztelyi, L., Culhane, J.L., Manoharan, P.K., Elliott, H.A.: 2007, CME propagation characteristics from radio observations. *Solar Phys.* **244**, 167. DOI.

Reiner, M.J., Kaiser, M.L., Plunkett, S.P., Prestage, N.P., Manning, R.: 2000, Radio tracking of a white-light coronal mass ejection from solar corona to interplanetary medium. *Astrophys. J.* **529**, L53. DOI.

Roberts, J.A.: 1959, Solar radio bursts of spectral type II. *Aust. J. Phys.* **12**, 327.

Robinson, P.A., Cairns, I.H.: 1998, Fundamental and harmonic emission in type III solar radio bursts - I. Emission at a single location or frequency. *Solar Phys.* **181**, 363. DOI.

Schmidt, J.M., Cairns, I.H., Gopalswamy, N., Yashiro, S.: 2016a, Coronal magnetic field profiles from shock-CME standoff distances. *J. Geophys. Res.* **121**, 9299. DOI.

Schmidt, J.M., Cairns, I.H., Xie, H., St. Cyr, O.C., Gopalswamy, N.: 2016b, CME flux rope and shock identifications and locations: Comparison of white light data, Graduated Cylindrical Shell model, and MHD simulations. *J. Geophys. Res.* **121**, 1886. DOI.

Shanmugaraju, A., Suresh, K., Vasanth, V., Selvarani, G., Umapathy, S.: 2018, Interplanetary type II radio bursts and their association with CMEs and flares. *Astrophys. Space Sci.* **363**, 126. DOI.

Sharma, J., Mittal, N.: 2017, On high and low starting frequencies of type II radio bursts. *Astrophysics* **60**, 213. DOI.

Sharma, J., Mittal, N., Tomar, V., Narain, U.: 2008, On properties of radio-rich coronal mass ejections. *Astrophys. Space Sci.* **317**, 261. DOI.

Sheeley, N.R., Howard, R.A., Michels, D.J., Koomen, M.J., Schwenn, R., Mühlhäuser, K.H., Rosenbauer, H.: 1985, Coronal mass ejections and interplanetary shocks. *J. Geophys. Res.* **90**, 163. DOI.

Shen, C., Liao, C., Wang, Y., Ye, P., Wang, S.: 2013, Source region of the decameter-hectometric type II radio burst: Shock-streamer interaction region. *Solar Phys.* **282**, 543. DOI.

Song, H.Q., Zhang, J., Cheng, X., Li, L.P., Tang, Y.Z., Wang, B., Zheng, R.S., Chen, Y.: 2019, On the nature of the bright core of solar coronal mass ejections. *Astrophys. J.* **883**, 43. DOI.

Su, W., Cheng, X., Ding, M.D., Chen, P.F., Ning, Z.J., Ji, H.S.: 2016, Investigating the conditions of the formation of a type II radio burst on 2014 January 8. *Astrophys. J.* **830**, 70. DOI.

Uchida, Y.: 1960, On the exciters of type II and type III solar radio bursts. *Publ. Astron. Soc. Japan* **12**, 376.

Vasanth, V., Umapathy, S.: 2013, A statistical study on CMEs associated with DH-Type-II radio bursts based on their source location (limb and disk events). *Solar Phys.* **282**, 239. DOI.

Vasanth, V., Chen, Y., Kong, X.L., Wang, B.: 2015, Investigation of the geoeffectiveness of CMEs associated with IP type II radio bursts. *Solar Phys.* **290**, 1815. DOI.

Vourlidas, A., Ontiveros, V.: 2009, A review of coronagraphic observations of shocks driven by coronal mass ejections. *AIP Conf. Proc.* **1183**, 139. DOI.

Vrsnak, B., Cliver, E.W.: 2008, Origin of coronal shock waves. Invited review. *Solar Phys.* **253**, 215. DOI.

Vrsnak, B., Magdalenic, J., Zlobec, P.: 2004, Band-splitting of coronal and interplanetary type II bursts. III. Physical conditions in the upper corona and interplanetary space. *Astron. Astrophys.* **413**, 753. DOI.

Warmuth, A.: 2007, Large-scale waves and shocks in the solar corona. In: Klein, K.L., MacKinnon, A.L. (eds.) *The High Energy Solar Corona: Waves, Eruptions, Particles*, *Lect. Notes Phys.* **725**, 107. DOI.

Warmuth, A., Mann, G.: 2005, A model of the Alfvén speed in the solar corona. *Astron. Astrophys.* **435**, 1123. DOI.

Wild, J.P., McCready, L.L.: 1950, Observations of the spectrum of high-intensity solar radiation at metre wavelengths. I. The apparatus and spectral types of solar burst observed. *Aust. J. Sci. Res., Ser. A* **3**, 387.